

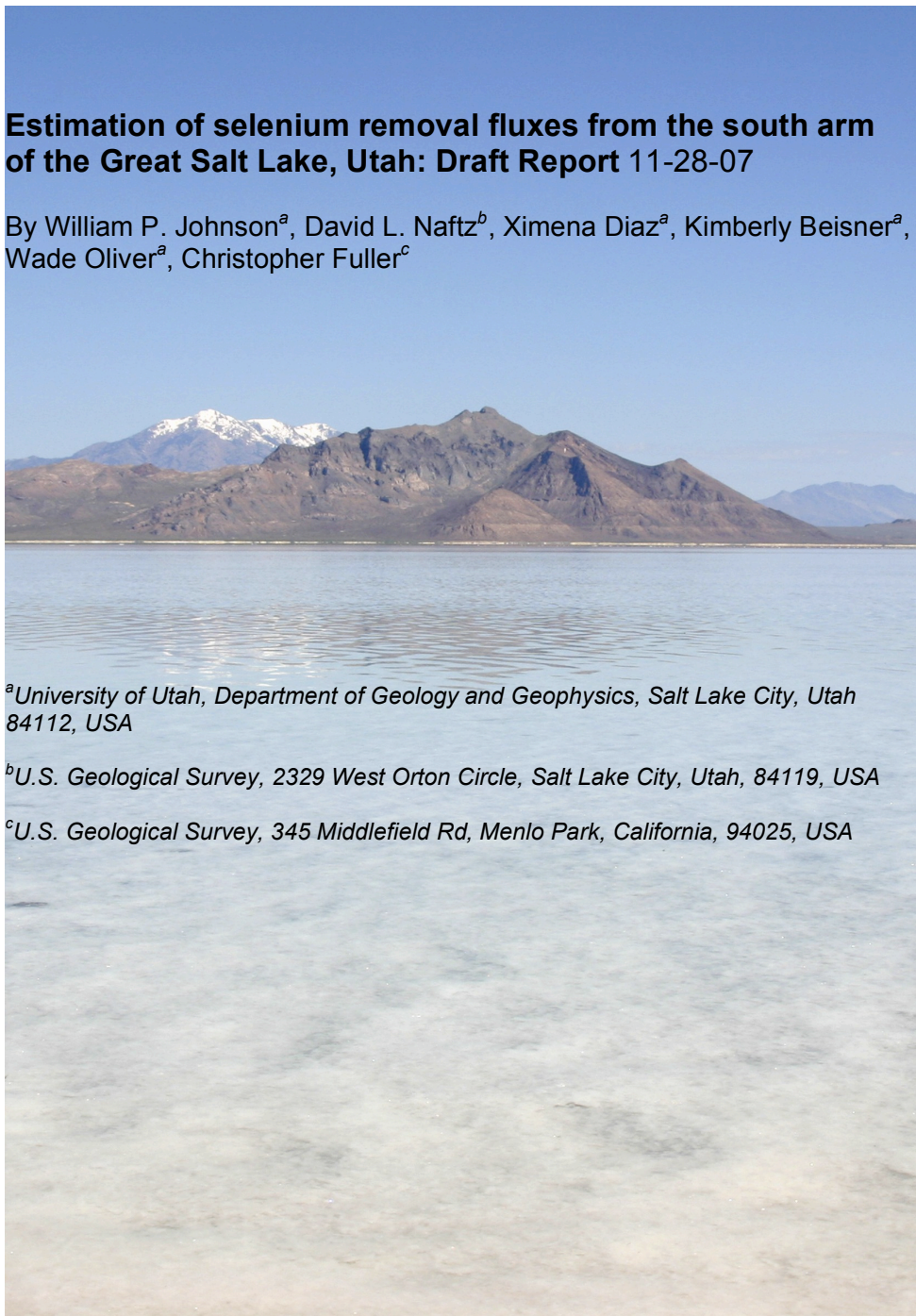
Estimation of selenium removal fluxes from the south arm of the Great Salt Lake, Utah: Draft Report 11-28-07

By William P. Johnson^a, David L. Naftz^b, Ximena Diaz^a, Kimberly Beisner^a,
Wade Oliver^a, Christopher Fuller^c

^a*University of Utah, Department of Geology and Geophysics, Salt Lake City, Utah
84112, USA*

^b*U.S. Geological Survey, 2329 West Orton Circle, Salt Lake City, Utah, 84119, USA*

^c*U.S. Geological Survey, 345 Middlefield Rd, Menlo Park, California, 94025, USA*



Ex **utive Summary**

Measurements were made during the period March 2006 through September 2007 to examine the existing distribution of selenium in the water and sediment of the south arm of the Great Salt Lake, and to measure Se fluxes between water, sediment, and the atmosphere at the Great Salt Lake. Results of these measurements are summarized in six sections below.

Great Salt Lake Characteristics

The average selenium (Se) concentration from May 2006 to July 2007 for unfiltered acidified (RA) samples was $0.64 \pm 0.28 \mu\text{g/L}$, whereas the filtered acidified (FA) samples showed an average Se concentration of $0.49 \pm 0.25 \mu\text{g/L}$ for the same period. Differences between total and dissolved Se concentrations showed that a significant but minor fraction of Se was carried in particulate phases, more so in the deep brine layer relative to the shallow brine layer, but in either layer, the Se mass was dominantly dissolved rather than particulate. In terms of temporal variation, increases in the measured total (RA) and dissolved (FA) Se concentrations were observed in both the deep and shallow brine layers during the period of the investigation ([Figure 7](#)), constituting a net increase ranging between 0.16 and $0.34 \mu\text{g/L}$ over the period of the investigation ([Naftz et al., 2007](#)).

Volatilization

The average concentration of volatile Se in the water column was 0.69 ng/L , but this measured concentration varied over a two orders of magnitude spatially and temporally. The measured volatile Se concentrations increased with depth for paired measurements in the shallow brine layer. Comparison of measured to estimated volatile Se flux showed reasonable agreement, indicating that Se flux to the atmosphere could be integrated from measured volatile Se concentrations, wind speeds, and water temperatures. The resulting estimated annual volatile Se flux to the atmosphere from the Great Salt Lake is 1890 Kg/yr . This estimate is considered accurate to within a factor of 7.7, yielding a potential range between 245 to $14,550 \text{ Kg/yr}$. The large range in estimated flux results from the spatial and temporal variability of volatile Se concentrations. Despite the variability, the results demonstrate that Se volatilization is the major mechanism of Se removal from the Great Salt Lake.

Downward Sedimentation

Downward sedimentation fluxes were highest where influenced by the Bear River inflow, and were lowest in the shallow brine layer at sites located near the northwest-southeast axis of the south arm. Notably, sediment accumulation rates in the deep brine layer were much greater than corresponding shallow layer sediment accumulation rates, suggesting that re-suspension accounted for most of the sediment accumulation at depth. The influence of re-suspension on sediment accumulation in the Great Salt Lake was also indicated by ^7Be analyses in sediment cores.

Permanent (Net) Sedimentation

The permanent Se removal flux via sedimentation was estimated at 248 Kg/yr , based on ^{210}Pb profiles from ten sediment cores in the south arm. This estimated

sedimentation flux is considered accurate to within a factor of two, yielding a range between 124 and 496 Kg/yr.

Re-suspension – Re-solubilization

Temperature readings from six depths at two sites in the south arm demonstrate periodic equilibration events consistent with temporary displacement of the deep brine layer via seiche transmission in the lake. This observation suggests that anoxic sediments are periodically placed into contact with oxic shallow brine layer, potentially leading to re-solubilization of Se from the anoxic sediment. Batch studies indicate that Se re-solubilization during these events yields negligible change in Se concentration in the water column.

Mass Balance

The combined sedimentation and volatilization fluxes total to about 2160 kg/yr (based on the geometric means). Comparison of volatilization to sedimentation flux demonstrates that sedimentation is NOT the major mechanism of removal of Se from the Great Salt Lake. Rather, volatilization is demonstrated to be the major mechanism of Se removal from the Great Salt Lake. These measured loss fluxes balance the measured annual load (1,450 Kg/yr) during the study period. The observed increase in total Se concentration during the period of the study indicates that most Se loads to the lake are not yet measured. However, it should be noted that the inefficiency of in-lake mixing processes complicates comparison of measured Se concentrations to measured Se loads and removal fluxes.

Table of Contents

Executive Summary.....	2
1. Introduction.....	5
2. Methods.....	6
2.1 Water column.....	6
2.2 Sediments.....	7
2.2.1 Sediment traps.....	7
2.2.2 Cores.....	8
2.2.3 Bed sediment samples.....	9
2.2.4 Freeze-drying, extraction, and chemical analyses.....	10
2.3 Analysis.....	11
2.3.1 Major and minor elements.....	11
2.3.2 Total Se analysis.....	12
2.3.3 Water.....	12
2.3.4 Sediments.....	12
2.3.5 Volatile Se analysis.....	12
2.3.6 Wind velocity, atmospheric temp., lake elevation, lake surface area.....	16
2.3.7 Total dissolved gas pressure, hydrostatic pressure, barometric pressure.....	18
2.3.8 Thermistor analysis.....	18
2.3.9 TOC analysis.....	20
2.3.10 Isotope analysis.....	20
2.3.11 Sediments.....	20
3. Results.....	22
3.1 Great Salt Lake characteristics.....	22
3.1.1 Water.....	22
3.1.2 TOC.....	23
3.1.3 Bed sediment.....	23
3.2 Volatile selenium flux.....	24
3.2.1 Volatile Se concentrations.....	24
3.2.2 Volatilization flux estimates.....	24
3.2.3 Direct measurement of volatilization flux.....	25
3.2.4 Integration of the volatile Se flux.....	26
3.3 Sedimentation fluxes.....	29
3.3.1 Downward sedimentation flux.....	29
3.4 Permanent sedimentation or net sedimentation.....	30
3.4.1 Mass accumulation rates.....	30
3.4.2 Downward sedimentation vs. net sedimentation.....	31
3.4.3 Estimation of Se removal by sedimentation.....	31
3.5 Re-suspension – Re-solubilization.....	33
3.5.1 Temperature stratification.....	33
3.5.2 Seiche.....	34
3.5.3 Mechanism of temperature equilibration events.....	34
3.5.4 Batch equilibration tests.....	36
3.6 Brine shrimp flux.....	!Error!Marcador no definido.
3.7 Mass balance.....	37
4. References.....	41

1. Introduction

Characterization of the existing distribution of selenium (Se) in the water and sediment of the south arm of the Great Salt Lake, and measurement of Se fluxes between water, sediment, and the atmosphere at the Great Salt Lake are motivated by the goal of setting a Se standard for the open waters of the Great Salt Lake.

The open waters of the GSL are protected for their current beneficial uses (Class 5) through the application of the narrative criteria clause. Existing EPA-promulgated numeric standards for inland lakes cannot be applied to the Great Salt Lake due to its highly individual nature, i.e. large, terminal, hypersaline, and meromictic (i.e. multiple, stable layers).

The development of an open water standard for Se requires a working knowledge of the biological significance of existing Se concentrations in the Great Salt Lake, as well as a working understanding of the likely changes in these concentrations over time given existing and proposed loads to the system. This “working knowledge” has been previously represented in a conceptual model (Johnson et al., 2006) that accounts for Se in various “stocks” in the system (e.g. water, sediment, biota) and the “flow” of Se between stocks (e.g., precipitation and settling, volatilization, and bioconcentration).

The conceptual model serves as the basis for five investigations conducted during the period April 2006 to October 2007. These investigations involved: 1) Characterization of Se concentrations and effects in avian species associated with the south arm of the Great Salt Lake; 2) Characterization of Se concentrations and effects in brine shrimp, seston, and benthic organisms in the south arm of the Great Salt Lake; 3) characterization of Se uptake kinetics in brine shrimp; 4) Determination of annual Se loads to the south arm of the Great Salt Lake; 5) Characterization of the distribution of Se in water and sediment and determination of selenium removal fluxes via sedimentation and volatilization in the south arm of the Great Salt Lake. This report describes findings of the 5th investigation.

2. Methods

2.1 Water column

Aqueous chemical conditions were characterized in the field at 19 locations across the main body of the Great Salt Lake (Figure 1). Four of these stations (2267, 2565, 2767 and 3510) were characterized at 7 to 13 depths (varying by station), ranging from 0.2 to 8 m depth below lake surface. The remaining stations were characterized at three depths (3, 6 & 8 m). Aqueous characteristics included temperature, conductivity, pH, oxidation-reduction potential (ORP), and dissolved oxygen (DO), as measured using a Hydrolab Troll 9000 (In-Situ Inc., Fort Collins, CO).

Samples for major and trace element analysis were collected in acid-rinsed polyethylene bottles from four stations (2267, 2565, 2767 and 3510). At two stations (2267 & 2767), samples were collected from two depths representing the shallow brine layer (0.2 m (both sites) and 4 m (2267) or 2.5 m (2767)). At the remaining two stations (2565 & 3510), samples were collected from three depths representing the shallow and deep brine layers and the interface between them (0.2, 8, and 6.5 m, respectively). Replicate samples (4 x 250 mL) were collected from each location using a peristaltic pump with acid-rinsed C-flex tubing (Cole-Parmer's Masterflex, Vernon Hills, IL). Two of the replicates were filtered (0.45 μ m pore size, capsule-type filter). All four replicates were stored on ice, acidified (trace metals grade nitric acid, 2 mL, 7.7 N), and transferred to a refrigerator. One each of the filtered-acidified and raw-acidified samples were sent to a contract lab (Frontier Geoscience, Seattle, WA) for total Se analysis as described below. The other replicates were stored at 4°C for major and trace elements analyses (Al, As, Ba, Ca, Cd, Co, Cr, Cu, Fe, K, Li, Mg, Mn, Mo, Na, Ni, Pb, S, Sb, Sc, Sr, Ti, Tl, U, V, Zn) via inductively coupled plasma mass spectrometry (ICP-MS) as described below.

At the 19 locations in Figure 1, analyses were performed for volatile Se concentrations and total dissolved gas pressure, at multiple depths (representing deep and shallow brine layers). Semi-monthly samples were taken at those locations and multiple depths in the south arm of the Great Salt Lake to explore temporal variations in volatile Se concentrations. Collection of volatile Se using the purge and cryo-focusing trap process was performed in-situ at the respective sampling sites on the lake in order to avoid any degradation of the water sample (as described in the Analyses section).

Direct measurements of volatilization of Se were taken at two primary (3510 and 2267) and one secondary (2565) location in the south arm of the Great Salt Lake. The flux measurements were taken concurrently with characterizations of the parameters used in estimating volatile Se flux: surface water temperature, wind velocity, and volatile Se concentration, in order to assess the accuracy of the predictive model.

At an additional twelve locations in the deep brine layer (Figure 1), samples were taken for total organic carbon (TOC) analysis (GS1, GS3, GS4, GS5, GS8, GS9, GS11, GS12, GS14, GS15, GS18, GS20).

At sites 2565 and 3510 (Figure 1), temperature was measured at 6 depths spanning the interface between the deep and shallow brine layers. Temperature was measured using thermistors (StowAway®, TidbiT™, model #89419) attached to the sediment trap cables. For site 2565, thermistor distances above the anchor were 1.75, 2.10, 2.45, 2.81, 3.15 and 3.51 meters. In August 2006, the chain at the base of the site 2565 trap was shortened by one meter to decrease the distance of each thermistor above the base by 1 meter. For site 3510, thermistor distances above the anchor were 1.86, 2.21, 2.61, 3.02, 3.38 and 3.73 meters. At both sites (2565 and 3510), thermistor spacing was increased (on September 28, 2006) to 0.5 m to yield distances above the anchor of 1.0, 1.5, 2.0, 2.5, 3.0 and 3.5 meters (Figure 2a). Thermistor readings were taken at 6-minute intervals, and were downloaded approximately monthly with an optical reader device that connects to a computer. Once the data had been offloaded from the thermistors, Boxcar® software was used to view the data and export data files to Excel.

2.2 Sediments

2.2.1 Sediment traps

2.2.1.1 Description

The sediment traps used for sampling in the Great Salt Lake consist of balanced pairs of detachable cylindrical acrylic sampling traps (72 mm internal diameter, 450 mm length) mounted in stainless steel holders located above their center of gravity to keep them vertical (Figure 2). The holders were attached to a stainless steel cable strung between a cement anchor and a buoy.

The traps were deployed at three sites representing three distinct locations in the main body of the Great Salt Lake (Figure 1). Site 2267 was located near the mouth of the Bear River, the largest contributor of flow to the lake (70% of inflows). Sites 2565 and 3510 represent northern and southern basins in the main body of the lake. At site 2267, the top of a sediment trap pair was placed at 2.8 m below the lake surface (Figure 2b), where the water depth was 4.1 m. At sites 2565 and 3510, where the water depths were 8.1 and 8.4 m, respectively, the trap pair tops were placed at two depths, approximately 3.7 m and 7 m below the lake surface (Figure 2c), corresponding to the shallow and deep brine layers, respectively.

2.2.1.2 Collection and processing of sediments

Sediments from sediment traps were collected approximately monthly starting March 3, 2006 for sites 2267 and 2565, and starting June 27, 2006 for site 3510.

After retrieving the sediment traps from the water, most of the water was drained using a peristaltic pump. The remaining water was swirled to make slurry, which was collected in 1-L polyethylene bottles and kept on ice until transfer to a refrigerator.

Processing involved filtering the slurry onto a Millipore vacuum filtration system (1.2 μm pore size, glass microfibre filter). The filter cake was freeze-dried, digested and analyzed as described below.

2.2.2 Cores

2.2.2.1 Collection and sub-sampling

Historical and contemporary sedimentation rates and sediment Se concentrations were investigated by analysis of sediment cores taken at various sites in the South Arm of the Great Salt Lake in order to estimate permanent Se removal by sedimentation.

Shallow cores (~6 cm) were taken at 20 sites (yielding quantifiable sedimentation rates in 13 sites) during June, 2007 across the south arm of the Great Salt Lake. A preliminary linear sedimentation rate was determined in each core based on ^{210}Pb decay at intervals of 0-1 cm and 4-5 cm using the CF-CS (constant flux-constant sedimentation) method (described below). Though these rates did not account for compaction of sediment, they were useful for determining relative differences in sedimentation rates, and were used as a guide to select the five additional deep coring sites occupied in 2007.

Deep core sediments were collected at sites 2267, 2565 and 3510 (Figure 1) during July, 2006 and in five additional locations during July, 2007. Each of the 2007 cores was sliced into a minimum of 10 1-cm increments. At site 2267 (total water depth of 4.1 m), one gravity core of 88 cm in length was recovered. The top ten centimeters were sliced in 2-cm intervals, whereas the remainder of the core was sliced in 3-cm intervals. At site 2565 (total water depth of 8.1 m), two gravity cores (32 and 35 cm) were collected. Both were sliced in 2-cm intervals. For site 3510 (total water depth of 8.4 m), two core samples were collected. A box corer was used to collect a 12.5-cm sediment core. This device was used to avoid compaction of this shallow core, in order to provide the best possible determination of age as a function of depth (and sedimentation rate). This sample was sectioned in-situ in 1-cm intervals. The core slices were placed into individual plastic containers and were stored on ice until transfer to a freezer. Also at site 3510, a gravity coring device was used to collect a 38-cm long core, which was sliced in 2-cm intervals. The 2007 cores were collected with a gravity core device, cut into 1-cm slices and processed in a similar manner as the 2006 cores.

All deep core slices were freeze-dried as described below and ground using a ceramic mortar and pestle. After grinding, the samples were homogenized by mechanical mixing and divided into four fractions.

The homogenized core slices were divided into four fractions. One fraction was analyzed for sedimentation rate using the CF-CS method for more precise determination of sediment mass accumulation rates (MAR) in these cores (at the USGS, Menlo Park, CA). In the CF-CS method, the natural logarithm of unsupported ^{210}Pb (dpm/g) in each 1-cm increment is plotted against the cumulative dry mass (g/cm^2)

of sediment. The decay constant for ^{210}Pb divided by the slope of the linear trendline on the above plot yields the sediment MAR in $\text{g}/\text{cm}^2/\text{yr}$.

In eight cores, the second fraction was sent to the contract lab (LET Incorporated, Columbia, MO) for Se analysis. To limit the influence of diagenetic processes acting on the upper sediments, only those values below 5 cm (the depth at which concentration generally stabilized) were included in calculating the average Se concentration for each core.

In three cores, the third fraction was analyzed for minor and major elements by ICP-MS at the University of Utah as described below. The fourth fraction was archived at room temperature.

Estimating Selenium Removal by Sedimentation

Holocene sediment thicknesses were estimated by Dr. David Dinter (University of Utah) by analysis of 30 Chirp (variable frequency) and Geopulse high-resolution seismic reflection transects (Dinter, 2007), as shown in the Results section. These Holocene thickness contours were plotted in ArcGIS along with the shallow core results in order to develop contours delineating qualitative zones of very high to very low sedimentation rates for the past ~10,000 years. Average MAR in each zone was determined by comparison of 10,000-yr sedimentation zones to the MARs from the eight deep cores, as shown in the Results section. The Se concentrations in the eight deep cores provided average sediment selenium concentrations for each zone.

With the Se concentration, mass accumulation rate, and area known for each of the sedimentation zones described above, the following equation was used to determine the permanent Se removal by sedimentation for each zone:

$$Se \text{ Removed} \left(\frac{\text{kg}_{\text{Se}}}{\text{yr}} \right) = Se \text{ Conc.} \left(\frac{\mu\text{g}_{\text{Se}}}{\text{g}_{\text{sed}}} \right) \times MAR \left(\frac{\text{g}_{\text{sed}}}{\text{cm}^2 \text{ yr}} \right) \times Area (\text{km}^2) \times 10 \left(\frac{\text{cm}^2 \text{ kg}_{\text{Se}}}{\text{km}^2 \mu\text{g}_{\text{Se}}} \right)$$

The sum of the sedimentation fluxes in each of the zones yielded the total mass of Se removed by sedimentation over the entire south arm.

2.2.3 Bed sediment samples

2.2.3.1 Collection and treatment

Thirty bed sediment samples were collected at 15 locations (ranging from 6.8 to 9.4 m in depth) in the main body of the Great Salt Lake using an Eckman dredge on May 31, June 2, 26 and 27, 2006 (Figure 1, GS sites). The sediment surface was typically coated with what appeared to be an organic-rich ooze. Hence, 10 ooze layer samples (top 1-2 cm) were taken at 12 locations (GS1, GS4, GS5, GS8, GS9, GS11, GS12, GS14, GS18, GS20) (two locations did not have an ooze layer: GS3 & GS15), using a

plastic spoon to scoop this surface off the collected sediment. Eight samples corresponded to composite sediments (mixture of ooze and underlying mineral sediment). The remaining 12 sediment samples corresponded to the mineral layer. Composite, ooze, and mineral layer samples were collected in glass jars and kept on ice until transfer to a refrigerator.

Each sample was subdivided in the laboratory and stored in pure water-rinsed plastic centrifuge tubes in a freezer. Bed sediment subsamples were sent to a contract lab (LET Incorporated, Columbia, MO) for Se analysis using proprietary digestion procedures. Bed sediment subsamples were also analyzed for major and trace elements (including Se) via ICP-MS at the University of Utah as described below. Prior to analysis, bed samples were thawed to allow drainage of water, and then were freeze-dried, digested and analyzed as described below.

2.2.3.2 Batch tests

Batch equilibration tests were performed to determine whether significant Se would be re-solubilized from anoxic bed sediment upon equilibration with shallow brine layer water (e.g. via re-suspension or displacement of the deep brine layer). Shallow brine layer water (15 g) collected from site 2267 in December 2006 was equilibrated with anoxic bed sediment (7.5 g) in a 50-ml plastic centrifuge tube. The equilibration test was performed for sub-samples from all 15 bed sediment sampling sites. In order to avoid direct addition of atmospheric oxygen to the sample, the bed sediment container was opened and a sub-sample was added to the shallow brine layer water in a nitrogen glove bag. In order to examine the influence of the availability of oxygen on Se re-mobilization into the shallow brine layer, two batch equilibration replicates were performed for each bed sediment sample; one with nitrogen, and the other with air, in the centrifuge tube headspace (25 ml). The centrifuge tubes were placed upright on a shaking table (130 rpm) for 24 hours. Following equilibration, centrifuge tubes were centrifuged at 5500 rpm for 3 minutes, and supernatant was removed and acidified to < pH2 by addition of 0.8% nitric acid by volume. Major and trace element concentrations were analyzed via ICP-MS. Equivalent batch experiments were performed on exposed shore zone sediments; however, these results are described in the report for the 4th project concerning Se loads to the south arm of the Great Salt Lake.

William P. Johson 11/1/07 4:31 AM
Comentario: We've provided information on Se release, and will provide information on release of other monitored elements (Kim Beisner)

2.2.4 Freeze-drying, extraction, and chemical analyses

Sediment samples were freeze-dried under vacuum using a liquid nitrogen trap. Wet and dry weights were recorded. Salt content was corrected based on water weight and salinity.

Extraction of metals from freeze-dried sediment (approximately 0.5 g) was performed serially in trace metal grade nitric acid (3 mL, 15.8 N) and trace metal grade hydrochloric acid (5 mL, 12 N) using a Savillex 60-mL teflon closed reactor heated by microwave oven at 50% power for 2.5 min per reactor. The extraction solution was

collected in a 50-mL centrifuge tube and made up to a volume of 50 mL with milliQ water. The mixture was centrifuged at 5000 rpm for 30 minutes. The supernatant was collected in a pure water-rinsed centrifuge tube while the sediments were collected in a glass Petri dish and dried at 110°C prior to weighing. For each 10th sample, a duplicate was treated via the extraction procedure and analyzed independently.

Elemental analyses of the extraction solutions were carried out using ICP-MS at the University of Utah Center for Water, Ecosystems, and Climate Sciences (CWECS) laboratory facility.

Sediments were analyzed for Se and 29 other major and minor elements (Ag, Al, As, Ba, Be, Ca, Cd, Co, Cr, Cu, Fe, K, Li, Mg, Mn, Mo, Na, Ni, P, Pb, S, Sb, Sc, Sr, Ti, Tl, V, U, Zn) using ICP-MS. Although Hg is another element of interest, it cannot be reliably measured in most aquatic systems using ICP-MS.

For sediment samples greater than 4 grams, a representative split was sent to a commercial analytical laboratory (LET Incorporated, Columbia, MO) for Se analysis.

2.3 Analysis

2.3.1 Major and minor elements

2.3.1.1 Water

ICP-MS analyses in water were carried out in an Agilent 7500 ce. Interferences were minimized by collision or reaction with gas in a collision cell. Se, As and Cr were analyzed using hydrogen gas in the collision cell, while analyses for the rest used helium as a collision cell gas. Indium (7 µg/L equivalent concentration) was used as internal standard. General conditions used in the ICP-MS for water sample analyses are presented in [Table 1a](#).

Dilution of Great Salt Lake samples was required to prevent salt accumulation and consequent decrease of ICP-MS signal. Major elements (Ba, Ca, Cl, K, Li, Mg, Na, S) were diluted 100:1 or 900:1 prior to being analyzed. Minor elements were diluted 50:1 or 30:1 prior to being analyzed. Methanol (3%) and HNO₃ (ultra high purity, 0.1%) was used as a dilution matrix. A synthetic Great Salt Lake matrix was used in the preparation of standards and quality control samples. The chemical recipe for this solution is given in [Table 1b](#).

Quality control was carried out using the US EPA Multi-Media, Multi-Concentration, Inorganic Analytical Service for Superfund (ILM05.3) for ICP-MS, released in February 2004 and upgraded in January 2007 ([Table 1c](#)). The samples used for QA/QC (quality assurance/quality control) included an initial calibration blank (ICB), initial calibration verification (ICV), CRQL check standard (CRI), continuing calibration verification (CCV), continuing calibration blank (CCB), and interference check sample (ICS). For each 10 samples, a duplicate, spike, spike duplicated, serial dilution, CCV, and CCB were run.

2.3.1.2 Sediments

As described below, sediment samples were freeze-dried, digested and analyzed by ICP-MS for 30 elements. Solution samples were diluted 20:1 using 3% methanol and 0.1% HNO₃ (ultra high purity) as a dilution matrix. The same matrix was used in the preparation of standards and quality control samples. The same QC/QC protocol used for analyses of water samples was used for sediment samples.

2.3.2 Total Se analysis

2.3.3 Water

2.3.3.1 Hydride generation

Frontier Geoscience (Seattle, WA) analyzed total Se in water by a hydride generation and atomic fluorescence spectrometry (HG-AFS).

2.3.4 Sediments

2.3.4.1 Hydride generation

Total Se in sediments was analyzed at LET Inc. (Columbia, MO) laboratory by hydride generation – atomic absorption spectrometry on acid-digested samples. Maximum detection limit for Se was 0.4 mg/Kg.

It should be noted that the sediments collected from the sediment traps had Se concentrations below the LET detection limit.

2.3.4.2 ICP-MS

Sediment samples were freeze-dried, digested and analyzed for total Se by ICP-MS at the CWECS laboratory facility. Samples were diluted 20:1 and analyzed as described above. Maximum detection limit for Se was 0.01 mg/Kg.

2.3.5 Volatile Se analysis

2.3.5.1 Water

2.3.5.1.1 Purge and cryo trap system

Collection of volatile Se from the water involved a cryo-focusing trap system (Figure 3a) following concepts used by researchers at the University of Pau in France (Amouroux and Donard, 1996).

The system consisted of a reactor (a modified desiccator) with a diffuser connected to a helium line. The reactor sparges 7 liters of hypersaline water. The vapor swept from the reactor moved via Teflon tubing to a glass water trap (-55°C, dry ice/ethanol) to remove water from the flowing vapor. The vapor then entered a glass trap (-196°C, liquid nitrogen) to trap the volatile compounds collected from the water. Studies demonstrate that the entire volume of water can be sparged at a helium flow rate of 300 mL/min for approximately 15 minutes. After collection, nitric acid was added to the glass trap to oxidize volatile Se compounds and convert them to their stable aqueous species. The closed trap was digested in a water bath at 75°C for 3 hours, and the solution was analyzed for Se by ICP-MS at the University of Utah CW ECS laboratory facility.

The purge and cryo-focusing trap system was calibrated with dimethyl selenide (DMeSe) (AlfaAesar, 99% purity), which is reported to be the most stable volatile Se compound in seawater (Amouroux et al., 2000). This system was tested in the laboratory using Great Salt Lake water spiked with pure dimethyl selenide. The analyzed spiked dimethyl selenide concentrations were equivalent to the expected value (within the 95% confidence limit) based on the calibration curve (Figure 3b). Since measurements of pure water yield apparent volatile Se concentrations of 0.04 ± 0.01 ng/L, the practical detection limit for volatile Se using the purge and trap system is 0.04 ng/L. These results demonstrate that the system can quantify volatile Se concentrations in the nanogram per liter (ng/L or ppt) range. This resolution is 100 to 1000 times greater than typical analyses used for aquatic contaminants. It should be noted that the regressed recovery of volatile Se was 25% due to losses in the system. Therefore, measured values were corrected for 25% recovery according to the regression on Figure 3b. The losses yielding the 25% recovery likely include partitioning to stainless steel, ceramic, glass and teflon surfaces in the chamber and tubing, and to epoxy sealant in holding the lid of the chamber (which was a modified dessiccator). Between samples, the entire system was thoroughly cleaned by rinsing five times with nitric acid (4 L, 2%) and deionized water (4 L). Tests demonstrated that volatile Se concentrations returned to background concentrations after cleaning. The calibration curve was used to correct the values measured in the field.

Laboratory tests were run using pure water and Great Salt Lake shallow brine water with and without spiking of DMeSe to determine the analytical. This error was determined to be 13%, which includes the error associated with the ICP-MS analyses.

2.3.5.2 Fluxes calculations, different temperatures and wind velocities

2.3.5.2.1 Models

To estimate the volatile Se flux from the Great Salt Lake to the atmosphere, several models are available in the literature. These models have been used for estimating fluxes in fresh and sea water.

The general equation for mass transfer flux for a volatile compound between two phases is defined in terms of the overall mass transfer velocity ($k_{ph1/ph2}$) and the

concentration gradient between the phases (Schwarzenbach et al., 2003). An expression for the volatile Se flux in the Great Salt Lake is given below with the assumption that mass transfer is kinetically controlled in the water phase, as opposed to mass transfer in the vapor phase being the kinetically limiting process.

$$\text{Flux} = ak_w (C_{\text{water}}^{\text{VSe}} - C_{\text{water}}^{\text{VSe,eq}}) = ak_w \left(C_{\text{water}}^{\text{VSe}} - \frac{C_{\text{air}}^{\text{VSe}}}{K'_{H_{\text{GSL}}}} \right) \text{ (mol/m}^2\text{/yr)}$$

where: a is a unit correction factor (= 0.24); k_w is the water transfer velocity in the air-water interface (cm/h); $C_{\text{water}}^{\text{VSe}}$ is the concentration of volatile Se in water (mol/m³); $C_{\text{water}}^{\text{VSe,eq}}$ is the equilibrium concentration of volatile Se in water (mol/m³); $C_{\text{air}}^{\text{VSe}}$ is the concentration of volatile Se in air (mol/m³); $K'_{H_{\text{GSL}}}$ is the dimensionless Henry's constant for volatile Se for the Great Salt Lake.

In our case, concentrations of volatile Se in the water have been measured. Concentrations of volatile Se in the air can potentially be measured; however, in the estimations below we assume this concentration to be zero.

2.3.5.2.1.1 Dimensionless Henry's constant correction

The dimensionless Henry's constant ($K'_{H_{\text{GSL}}}$) and the water mass transfer velocity in the air-water interface (k_w) were determined using empirical models from the literature. These models are based on wind velocity, water temperature, viscosity and diffusivity of the volatile species. The viscosity, diffusivity, and dimensionless Henry's constant each require corrections for the salinity of the Great Salt Lake, which is 3-5 times greater than that of the ocean.

An equation to estimate the dimensionless Henry's constant for DMeSe as a function of temperature was developed by Guo et al. (2000), whereas a salinity correction was provided by Schwarzenbach et al. (2003), yielding:

$$K'_{H_{\text{GSL}}} = 0.0248 \exp(0.0418T) * 10^{K^s[\text{salt}]_{\text{tot}}}$$

where K^s is the salinity constant, and $[\text{salt}]_{\text{tot}}$ is the total molar concentration of salt. Dimethyl selenide (DMeSe) is the most important volatile Se compound found in air; and in fresh and saline waters (Atkinson et al., 1990; Neumann, 2003; Tessier et al., 2003), and therefore is an appropriate species on which to base our estimations. The K^s for DMeSe was not available from the literature, whereas a value for dimethyl sulfide (DMeS) was available, and was used on the basis of its similarity to DMeSe (Amouroux, 1995).

2.3.5.2.1.2 Water transfer velocity - Estuarine model

To calculate the water transfer velocity, an approximation used in the Hudson estuary by Clark et al. (1995), corrected for the Schmidt number according to the boundary layer model (Schwarzenbach et al., 2003). This so-called Estuarine model is as follows:

$$k_w(cm/h) = \left(\frac{Sc}{600}\right)^{-1/2} (2 + 0.24u_{10}^2) \text{ for } u_{10} > 5 \text{ m/s}$$

$$k_w(cm/h) = \left(\frac{Sc}{600}\right)^{-2/3} (2 + 0.24u_{10}^2) \text{ for } u_{10} \leq 5 \text{ m/s}$$

where Sc is the Schmidt number, and u_{10} is the wind velocity measured 10 m over the surface of the lake.

Saltzman et al. (1993) defined a Schmidt number for DMeS as a function of water temperature (°C) and corrected for the sea water salinity (via coefficients) as follows:

$$Sc_{DMeS}^{sea\ water} = 2674.0 - 147.12T + 3.726T^2 - 0.038T^3$$

2.3.5.2.1.3 Water transfer velocity - modified Liss and Merlivat model

An alternative approach is provided by the modified Liss and Merlivat model (Livingstone and Imboden, 1993; Liss and Merlivat, 1986), the results of which largely corroborate the Estuarine model. This model, which was also corrected for the Schmidt number according to the boundary layer model (Schwarzenbach et al., 2003), defined three wind velocity regimes:

$$k_w(cm/h) = \left(\frac{Sc}{600}\right)^{-2/3} (0.65 * 3.6 * u_{10}^2) \text{ for } u_{10} < 4.2 \text{ m/s}$$

$$k_w(cm/h) = \left(\frac{Sc}{600}\right)^{-1/2} (0.79u_{10} - 2.68) * 3.6 \text{ for } 4.2 \text{ m/s} < u_{10} < 13 \text{ m/s}$$

$$k_w(cm/h) = \left(\frac{Sc}{600}\right)^{-1/2} (1.64u_{10} - 13.69) * 3.6 \text{ for } u_{10} > 13.6 \text{ m/s}$$

2.3.5.2.1.4 Diffusive flux

The diffusive flux can be calculated assuming that diffusion is the limiting mass transfer process, as follows:

$$J = D_e \frac{\Delta C}{\Delta x}$$

where: J is the diffusive flux ($\text{g}/\text{cm}^2/\text{yr}$); D_e is the effective diffusion coefficient (cm/s), ΔC is the concentration gradient (ng/L); and, Δx is the difference in depth (m).

The diffusion coefficient for DMeSe can be calculated using the diffusion coefficient for DMeS as function of temperature, corrected for sea water, according to [Saltzman et al. \(1993\)](#):

$$D_{DMeSe} \approx D_{DMeS} = 0.0192 \exp(-18.1/RT)$$

where: R is the gas constant ($\text{kJ}/\text{mole K}$) and T is the temperature (K)

2.3.6 Wind velocity, atmospheric temperature, lake elevation, lake surface area

2.3.6.1 Wind velocity and atmospheric temperature

Wind velocity and atmospheric temperature data from January 2006 to August 2007 were obtained from the MesoWest station at Hat Island. Weekly surface water temperatures were obtained using AVHRR (advanced very high resolution radiometer). The AVHRR is a scanner mounted on National Oceanic and Atmospheric Administration (NOAA) polar-orbiting satellites for measuring visible and infrared radiation reflected from vegetation, cloud cover, shorelines, water, snow, and ice. (ESRI Support Center, <http://support.esri.com/index.cfm?fa=homepage.homepage>). The data were obtained for the period January 2006 to December 2006, from the Department of Meteorology at the University of Utah. Comparisons were made between the AVHRR data (January 2006 to December 2006) and thermistor measurements in Gunnison Bay (January 2006 to August 2007) to ensure that the AVHRR data correctly represented water surface temperature during the period of study ([Figure 3c](#))

The estimated error for wind velocity measurement is 2.5 m/s ([Horel, 2007](#)). The estimated error for temperature measurement from an AVHRR is $0.5 - 1^\circ\text{C}$ ([Crosman and Horel, 2006](#)).

2.3.6.2 Lake elevation and lake surface area

Lake elevation data were obtained from the USGS gage at the Saltair boat harbor. Surface area of the lake, used to calculate the cumulative volatile Se flux from the lake, was corrected for lake elevation according the data summarized by [Baskin \(2005\)](#). Water-surface elevations reported at the USGS Great Salt Lake gages are considered to be accurate within ± 0.10 foot of the datum in use (<http://ut.water.usgs.gov/gsl%20corr/gslcorrection.htm>).

2.3.6.3 Direct measurements of volatilization

Direct measurements of volatilization of Se were taken at two primary locations (3510 and 2267) and one secondary location (2565) in the south arm of the Great Salt Lake. The flux measurements were taken concurrently with characterizations of the

parameters used in estimating volatile Se flux: surface water temperature, wind velocity, and volatile Se concentration, in order to assess the accuracy of the predictive model.

An emission isolation flux chamber (St. Croix Sensory, Inc.) was used to collect volatilized Se from the surface of the lake (Figure 4a). The bottom of the stainless steel chamber is a cylinder that circumscribes a capture area for volatile compounds. Helium gas was released from a compressed helium tank and swept through the chamber (while it floated on the lake surface) to drive volatile gases coming from the lake into a cryo-trap. The sweep rate was set to approximately 3 L/min to prevent accumulation of volatilized Se (and other gases) within the chamber. A constant sweep rate was used in lieu of variable rate matching environmental conditions because studies have shown that high sweep rates can induce convection in the water column and subsequently bias flux results high (Card et al., 2002). A sweep rate of 3 L/min corresponds to approximately 1 chamber volume being swept every 6 min and is consistent with the manufacturer's recommendations.

The gas mixture in the chamber was then pumped (Universal 44XR Single Pump, SKC West Inc.) at an equivalent rate through Teflon tubing to a glass finger-trap in acetone/dry ice slush (-20°C) to remove any water vapor. Downstream of the water trap, volatile Se was cryo-focused onto glass wool in a finger-trap held at -170°C by liquid nitrogen and a Watlow PID temperature controller connected to a temperature sensor (PT-103-AM Platinum RTD, Lakeshore Cryotronics, Inc.) and cartridge heater (3039-002, Cryogenic Control Systems, Inc.). Figure 4b depicts the apparatus used to hold the glass finger-trap in the liquid nitrogen. Designed with the assistance of Dr. Kip Solomon (University of Utah) and Erwin McPherson (University of Utah), the device was placed in a Dewar flask filled with liquid nitrogen. The "heat" of the liquid nitrogen was conducted through the brass rod to the copper block and tube surrounding the finger-trap. The length of brass rod necessary for optimal temperature controller performance was determined experimentally to be 1 cm, at which point the cartridge heater embedded in the copper block was activated approximately 25% of the time. The stainless steel shield prevented any direct contact between the liquid nitrogen and the copper block and tube.

After a substantial sampling time (typically between 1.5 and 3 hours), the sample in the cryo-trap was acidified with 5 mL of 20% nitric acid to stabilize volatile Se compounds as oxidized aqueous species. The sealed trap was then digested in a water bath at 75°C for 3 hours and analyzed for Se by ICP-MS at the University of Utah CC-ICP-MS facility. The resulting measured concentration was then converted to a mass of Se and divided by the area under the flux chamber (0.13 m²) and the period of sampling in order to yield a flux rate.

Wind velocity measurements used for developing predicted fluxes were taken at 3 meters above the water surface using a Kestrel 1000 Wind Meter. These measurements were then projected to a height of 10 meters by the method described by Wind Energy Department of Risoe National Laboratory and Det Norske Veritas (2001) for use in flux prediction calculations. Surface water temperature and volatile Se

concentration measurement techniques are described in sections 2.1 and 2.4.5.1, respectively.

To ensure that the sampling system was operating properly, tests were performed to quantify the background level of Se, examine response of the system to qualitative changes in volatilization rate, and verify reproducibility of measurements. Three flux samples were taken in the laboratory by placing the chamber over a nitric acid-washed pan filled with pure water (Milli-Q) to determine the background “flux” that is measured in a pure sample. All background samples were low, with a mean of 1.60 ng/m²h and a maximum of 2.67 ng/m²h. To test response of the system, two more samples were taken at Saltaire marina for 30 minutes each. During the first sampling, a diffuser hanging 1 m below the surface bubbled helium through the water column into the flux chamber to produce a high flux rate. For the second sample the diffuser was turned off, producing a low flux rate. Analyses yielded an order of magnitude higher flux rate for the first sample relative to the second, indicating that the system responded appropriately. Finally, reproducibility was demonstrated by two 2-hour samples taken during the same day at site 2267. The results showed similar Se flux rates with a slightly higher flux rate corresponding to the sample that was taken under conditions of increased surface chop.

2.3.7 Total dissolved gas pressure, hydrostatic pressure, barometric pressure

2.3.7.1 Water

Total dissolved gas pressures were measured at 12 locations (GS1, GS3, GS4, GS5, GS8, GS9, GS11, GS12, GS14, GS15, GS18, GS20) and 6 depths (between 1.5 and 8 m) in the main body of the Great Salt Lake (Figure 1) by using a total dissolved gas (TDG) sensor (In-Situ Inc., Fort Collins, CO). The TDG probe needed at least 7 minutes for stabilization. The probe was zeroed at the lake surface before starting to measure the total dissolved gas pressure. TDG measurements were achieved each two months from May 31 to November 17, 2006. Hydrostatic and barometric pressure were measured at the same locations, depths and times given above, using a Hydrolab Troll 9000 (In-Situ Inc., Fort Collins, CO).

All TDG measurements made during spring, 2006 were well below hydrostatic pressure indicating insignificant exsolution of gas (including volatile Se), or exsolution of gas in discreet zones not corresponding to the TDG sites. The TDG measurements were discontinued in summer, 2006.

William P. Johnson 11/1/07 4:48 AM
Comentario: The data for July 2006 are available in Excel spreadsheets if needed.

2.3.8 Thermistor analysis

2.3.8.1 Lake Mixing

2.3.8.1.1 Thermal mixing

Temperature equilibration events in the water column may represent genuine mixing of the deep and shallow brine layers. Complete mixing or homogenization of the water

column should yield an intermediate temperature between the two temperatures of the stratified column.

The expected intermediate temperature can be determined from an energy balance, under the assumption that despite density and temperature differences among water column strata, the specific heats of these strata are equal. Since heat energy lost by one layer must equal the heat energy gained by the other layer, the intermediate temperature can be determined from the mass (m), specific heat (c), and temperature difference between the initial (T_1 and T_2) and final (T_3) temperatures for both strata:

$$m_1c(T_1 - T_3) = m_2c(T_3 - T_2)$$

Substituting density and volume for masses of the two water column strata, and considering a water column with a given cross sectional area with heights h_1 and h_2 for the strata:

$$\rho_1h_1(T_1 - T_3) = \rho_2h_2(T_3 - T_2)$$

The intermediate temperature can be determined as follows:

$$T_3 = \frac{\rho_1h_1T_1 + \rho_2h_2T_2}{\rho_1h_1 + \rho_2h_2}$$

For example, on June 14 the temperature of the deep brine layer was 16°C and the temperature of the shallow brine layer was 21°C and the thermal mixing of these two layers would yield:

$$T_3 = \frac{1.10 \frac{\text{g}}{\text{cm}^3} (6 \text{ m})(21^\circ\text{C}) + 1.16 \frac{\text{g}}{\text{cm}^3} (2 \text{ m})(16^\circ\text{C})}{1.10 \frac{\text{g}}{\text{cm}^3} (6 \text{ m}) + 1.16 \frac{\text{g}}{\text{cm}^3} (2 \text{ m})}$$

$$T_3 = 19.7^\circ\text{C}$$

2.3.8.2 Seiche periodicity

A seiche is a prolonged oscillating wave in a body of water initiated by atmospheric effects such as wind. The period of an internal seiche is related to the length of the lake (l) and the physical characteristics of the layers within the lake. In the Great Salt Lake, the layering (density stratification) is defined by salinity (deep and shallow brine layers) rather than temperature. The characteristics of the layers, epilimnion (e) and hypolimnion (h), are thickness (z) and density (ρ) (Wetzel, 2001).

$$t = \frac{2l}{\sqrt{\frac{g(\rho_h - \rho_e)}{\frac{\rho_h}{z_h} + \frac{\rho_e}{z_e}}}}$$

2.3.9 TOC analysis

2.3.9.1 Water

Water samples for total organic carbon (TOC) analysis were collected in acid-rinsed amber glass 250-mL bottles from the deep brine layer at 12 stations (GS1, GS3, GS4, GS5, GS8, GS9, GS11, GS12, GS14, GS15, GS18, GS20) (Figure 1). Samples were collected from each location using a peristaltic pump with acid-rinsed C-flex tubing (Cole-Parmer's Masterflex, Vernon Hills, IL), stored on ice and transferred to a refrigerator. TOC analysis were carried out at the U of U CW ECS laboratory facility using a TOC-5000 (Shimadzu, Columbia, MD) where water samples were analyzed sequentially for total carbon (TC) and inorganic carbon (IC), the TOC being the difference between TC and IC. In both analyses, the carbon contained in the sample was converted in CO₂ and analyzed by an infrared CO₂ analyzer. For the TC, the sample was heated at 680°C, while for the IC, the sample was acidified with H₃PO₄ (25%). QC samples included a duplicate, spike, check standard, spike standard, and a blank.

2.3.9.2 Sediments

TOC analyses in 31 bed sediment samples were carried out by LET Inc. (Columbia, MO) by using a LECO combustion carbon analyzer, based on National Soil Center Method 4H2. Sediment samples were heated in the combustion chamber in an atmosphere of pure oxygen, which converted the organic carbon in the sample into carbon dioxide gas. The quantity of carbon dioxide gas evolved from the sample was measured by an infrared CO₂ analyzer and automatically converted into a percent carbon value for the sample.

2.3.10 Isotope analysis

2.3.11 Sediments

Subsections of the freeze-dried sediment cores were analyzed at the U.S. Geological Survey (Menlo Park, CA) for ²¹⁰Pb, ²²⁶Ra, ²³⁴Th, ⁷Be, and ¹³⁷Cs activities for determination of sediment accumulation rates. Wet and dry weights were recorded to determine water content of sediment. Sediment bulk density was assumed to be 2.6 g/cm³. Sediment dry weights were corrected for salt content of sediment porewater assuming a salinity of 171 g/L (17.1 %). The assumed salinity value was based on

averaging measured salinity values of the deep brine layer obtained during late Summer and Fall, 2006.

Activities of total ^{210}Pb , ^{226}Ra , ^{234}Th , ^7Be , and ^{137}Cs were measured simultaneously by gamma spectrometry based on previously published methods (Van Metre et al., 2006; Fuller et al., 1999). Subsamples of dried sediment samples were sealed in 7-mL scintillation vials and counted using a high-resolution intrinsic germanium well detector. The upper 3 cm of the core was counted within two weeks of collection for determining ^7Be and unsupported ^{234}Th (half lives 53 and 24 days, respectively) as indicators of recent sediment deposition and reworking by mixing or resuspension processes.

^{210}Pb activity as a function of depth in the sediment provides an estimate of the sedimentation rate. ^{210}Pb in core sediments results from the decay of two isotopes: ^{222}Rn (referred to as unsupported lead) and the long-lived ^{226}Ra (referred to as supported lead). ^{222}Rn decays in the atmosphere to ^{210}Pb , and is deposited onto the lake surface where it becomes associated with settling particles and it is deposited in the accumulating sediment. ^{210}Pb has a half-life of 22.3 years; hence, the rate of ^{210}Pb decrease with depth corresponds to the rate of burial. However, another source of ^{210}Pb is present in the sediment (^{226}Ra) and must be accounted for.

The supported ^{210}Pb activity, defined by its long-lived progenitor, ^{226}Ra activity, was determined on each interval from the 352 KeV and 609 KeV gamma emission lines of ^{214}Pb and ^{214}Bi daughters of ^{226}Ra , respectively. Supported ^{234}Th activity was determined by re-analyzing the samples 5 months later, after decay of unsupported ^{234}Th activity. Self-absorption of the 46 KeV ^{210}Pb and 63 KeV ^{234}Th gamma emission lines was corrected using the attenuation factor for each counting vial that was calculated via an empirical relationship between self absorption and bulk density (Cutshall et al., 1983). Self-absorption of the ^{214}Pb , ^{214}Bi , 474 KeV ^7Be and the 661.5KeV ^{137}Cs gamma emission lines was negligible. Detector efficiency for each isotope was determined from NIST traceable standards. NIST and IAEA reference materials were used to check detector calibration. The reported uncertainty in the measured activity was calculated from the random counting error of samples and background spectra at the one standard deviation level, and was typically within $\pm 10\%$. The measured activities of replicate analyses of material from the same interval agreed to within $\pm 15\%$.

Sedimentation rate was determined using the constant flux–constant sedimentation rate (CF-CS), method of Appleby and Oldfield (1992). The CF-CS method assumes a steady state accumulation of sediments and a constant unsupported ^{210}Pb activity per gram of depositing sediment particles.

3. Results

3.1 Great Salt Lake characteristics

3.1.1 Water

3.1.1.1 Spatial and depth variation

Total Se concentrations in water samples (raw acidified) show no apparent spatial trend (Figure 5), as represented by the data collected for May, 2006. The lack of a spatial trend was apparent in all other months sampled (Table 2).

The average Se concentration from May 2006 to July 2007 for unfiltered acidified (RA) samples was 0.64 ± 0.28 $\mu\text{g/L}$, whereas the filtered acidified (FA) samples showed an average Se concentration of 0.49 ± 0.25 $\mu\text{g/L}$ for the same period of time. The geometric means for Se were 0.60 ± 0.31 $\mu\text{g/L}$ and 0.45 ± 0.21 $\mu\text{g/L}$ for all RA and FA water samples, respectively, for the same period of time. The medians for RA and FA water samples were 0.64 and 0.46 $\mu\text{g/L}$, respectively (Table 2d), indicating a limited number of outliers. Quartile analysis for outliers indicates that the value obtained for site 2767 during June, 2007 (2.77 $\mu\text{g/L}$) corresponds to an extreme outlier, although it does reflect the trend of increasing total Se concentration during the period of the study (described below). Table 2 includes arithmetic and geometric means, median, standard deviation, and lowest and highest values for Se, calculated for each site (2267, 2767, 2565 and 3510).

In terms of depth, the major changes in water chemistry coincided with transition to the deep brine layer, where dissolved oxygen (DO), oxidation-reduction potential and pH decreased, conductivity increased and temperature increased or decreased depending on season (Figure 6).

Total Se (RA) concentrations also changed dramatically upon transition from the shallow to the deep brine layer (Figure 7c), either increasing or decreasing with no apparent relationship to season. In contrast, the vast majority of dissolved Se (FA) concentrations decreased upon transition from the shallow to the deep brine layer. These results indicate that particulate phases (if defined as RA minus filtered acidified, or FA) bear a significant but minor fraction of the Se mass in these samples.

Results for trace metals other than Se are shown in Table 3 and Figure 8. Notably, total As concentrations averaged 147 ± 6.3 $\mu\text{g/L}$ (with a geometric mean of 147 $\mu\text{g/L}$ and a median of 147 $\mu\text{g/L}$) in the shallow brine layer (Table 3 a & b). Total As concentration in the deep brine layer was 163 ± 16.7 $\mu\text{g/L}$ (with a geometric mean of 163 $\mu\text{g/L}$ and a median of 162 $\mu\text{g/L}$) (Table 3 c & d). Elements such as Al, Fe, Mn, Mo, and Pb showed significantly higher concentrations in the deep brine layer relative to the shallow brine layer (Figure 8 a & b). Particulate concentrations of some trace metals (Pb, Mo, Cu, Fe, Co, Ni, Zn, Ti, V) tended to be higher in the deep brine layer relative to

the shallow brine layer (Figure 9), possibly reflecting the formation of sulfide particulates and increased adsorption under the reduced conditions in the deep brine layer.

3.1.1.2 Temporal variation

In terms of temporal variation, increases in the measured total (RA) and dissolved (FA) Se concentrations (measured at Frontier Geosciences, Inc.) were observed in both the deep and shallow brine layers during the period of the investigation (Figure 7), constituting a net increase ranging between 0.16 and 0.34 $\mu\text{g/L}$ in the Great Salt Lake (Naftz et al., 2007).

William P. Johnson 10/28/07 12:45 PM

Comentario: Present UU data for corroboration? Harry says yes.

3.1.2 TOC

3.1.2.1 Spatial and temporal variations

Concentrations of total organic carbon (TOC) in the deep brine layer showed no spatial trend, as shown for June, 2006 (Figure 10). The lack of a spatial trend was observed for all other months. The TOC concentration remained constant over the sampling period, demonstrating no temporal variation (TOC averaging approximately 95 mg/L) (Figure 10).

3.1.3 Bed sediment

3.1.3.1 Se concentrations

3.1.3.1.1 Spatial variation

Total Se concentrations in bed sediment samples showed no spatial variation in either the ooze or mineral layer, or in the composite of the two (Figure 11).

At 8 of 10 sites where ooze was present, the Se concentration in the mineral layer was greater than the corresponding Se concentration in the ooze. The average Se concentration in the ooze layer was 0.83 ± 0.36 mg/Kg, whereas the average Se concentration in the mineral layer was 1.19 ± 0.22 mg/Kg.

TOC concentrations in bed sediment showed no spatial trend for any of the sediment samples retrieved (ooze, mineral layer, and composite) (Figure 12). Average TOC concentrations in the ooze and mineral layers were not significantly different, $4.46 \pm 2.1\%$ versus $3.65 \pm 1.5\%$, respectively.

Se concentrations in the bed sediments showed weak direct correlation with TOC concentrations for the ooze and the composite samples (Figure 13), with r^2 values around 0.5 (excepting the outlier at %TOC = 9.8). Se concentrations in the mineral layer samples showed no correlation with TOC concentrations.

3.2 Volatile selenium flux

3.2.1 Volatile Se concentrations

3.2.1.1 Spatially and with depth

Concentrations of volatile Se showed no spatial trend in the main body of the lake (Figure 14). Volatile Se concentrations increased with depth in the shallow brine layer (Figure 15a), for all sampling periods and sites where multiple depths were measured in the shallow brine layer. Volatile Se concentrations for depths below 5 to 6.5 m apparently decreased with depth, for all sampling periods and sites where multiple depths were measured (Figure 15b).

3.2.1.2 Temporal

The average volatile Se concentrations in water were reduced during the winter and elevated during spring, summer, and fall (Figure 16a and Table 4 a-c), coincident with warmer temperatures and increased primary productivity. During the course of the investigation, average concentrations (across the entire lake and entire water column) of volatile Se ranged from 2.4 ± 2.6 ng/L in September 2006 to 0.31 ± 0.47 ng/L in early December 2006 and 6.9 ± 6.9 ng/L in July 2007. This temporal trend is also reflected in the two-depth plots and three-depth plots shown in Figure 15a for the shallow brine. The same temporal trend occurred in the deep brine layer (Figure 15b).

The decrease in volatile Se concentrations in the shallow brine layer during winter 2006 corresponded to decreased temperature, and decreased primary productivity, which can be expected since phyto- and zoo-plankton are the expected main producers of volatile Se (Amouroux and Donard, 1996).

The average volatile Se concentration from September 2006 to August 2007 was 3.0 ± 4.4 ng/L. This value represents 0.6% of the average total Se concentration in the water column. Although this fraction seems negligible, its significance depends on the residence time of volatile Se in the lake. For example, water vapor represents only 0.001% of the global water budget whereas the great importance of water vapor (clouds) in transferring water across the surface of earth is undeniable, and arises from the short residence time of water in the vapor phase. The flux of Se from the lake to the overlying atmosphere must be known in order to assess its significance.

3.2.2 Volatilization flux estimates

Recalling that a near-surface volatile Se concentration gradient was observed (Figure 15), a diffusive flux was calculated assuming that diffusion is the limiting mass transfer process. The estimated diffusive flux was calculated for temperatures and concentration gradients observed in the lake (Table 5). The average diffusive flux yielded 3.9×10^{-12} g Se/cm²/yr, which translates to 7.3×10^{-2} Kg/yr. This extremely small

flux would represent the quiescent lake, which we believe is far too conservative a condition for this shallow large surface area lake. Furthermore, such a low volatilization flux is not consistent with observed Se concentrations in the Great Salt Lake, as described below.

The estimated water transfer velocities corresponding to wind-driven mixing (both models) are shown in [Table 6a](#). The volatile Se fluxes were estimated using an average volatile Se concentration of 3 ng/L, and the water transfer velocities corresponding to wind velocities of 5 and 25 miles per hour. Assuming a negligible volatile Se concentration in the overlying air, the corresponding volatile Se fluxes from the lake are shown in [Table 6a](#).

The estimated volatile Se fluxes range from 4.2×10^{-8} or 2.4×10^{-8} g Se/cm²/yr under cold, low-wind conditions to 8.2×10^{-7} or 5.6×10^{-7} g Se/cm²/yr under hot, high-wind conditions. This flux can be converted to a mass transfer rate by multiplying the known surface area of the lake (1842 km²) ([Baskin, 2005](#)). **The estimated Se mass transfer rates via volatilization range from 766 or 450 Kg/yr under cold, low-wind conditions to 15,030 or 10,395 Kg/yr under hot, high-wind conditions.**

3.2.3 Direct measurement of volatilization flux

The results of measured volatile Se fluxes from Great Salt Lake are shown in [Table 6b](#) along with the corresponding predicted flux rates (Estuarine model) and input variables (wind velocity, surface water temperature, surface volatile Se concentration). Measured fluxes ranged from 2 to 20 ng/m²h in the 5 samples with average wind velocities of 1 to 4 m/s, water temperatures of 20 to 28°C, and volatile Se concentrations of 0.05 to 4.4 ng/L.

The measured volatile Se fluxes were highly sensitive to near-surface volatile Se concentrations. For example, despite similar wind and wave conditions, samples 1C and 2C yielded volatile Se fluxes of 2.08 and 20.13 ng/m²h corresponding to measured near-surface volatile Se concentrations of 0.05 and 1.43 ng/L respectively.

Measured volatile Se fluxes did not change appreciably with changes in wind speed under the relatively calm conditions examined. For example, in two samples taken on 5/24/2007 to show reproducibility, measured flux rates were 10.7 and 8.0 for average wind velocities at 10 meters above the water surface of 5.1 and 6.7 m/s respectively. Though counterintuitive, the surface roughness during the first sample was significantly higher than the second resulting in the slightly higher flux rate for the first (assumes constant volatile Se concentration and water temperature). This observation is consistent with the fact that surface matrix effects, rather than wind speed, dominate liquid-to-atmosphere fluxes on liquid surfaces ([Schmidt, 2007](#)). Although increasing wind can increase surface roughness of a water body, the extent of convection also depends on wind direction and surrounding geography.

A plot comparing the measured volatilization rates to the Estuarine model-predicted rates is shown in [Figure 16b](#), where it is observed that 3 of the 5 measured fluxes

correlated well with the Estuarine model predictions. One of the measured fluxes was approximately an order of magnitude below the predicted flux, whereas another was an order of magnitude high relative to the predicted flux. The cause of these discrepancies is unknown; however, as volatile Se flux monitoring continues the degree of correspondence between measured and predicted fluxes should become clearer.

The data collected to date suggest that use of Estuarine model-predicted volatile Se fluxes, based on measured aqueous near-surface volatile Se concentrations, is appropriate for estimation of the annual volatile Se flux from the Great Salt Lake.

William P. Johnson 11/1/07 5:25 AM
Comentario: This will be updated (Wade Oliver and Ximena Diaz)

3.2.4 Integration of the volatile Se flux

A more useful estimation of annual Se flux is provided by integration of calculated volatile Se fluxes using recorded wind and temperature data. The volatile Se flux estimates from the Estuarine model were integrated over time using measured wind velocities (10 m above lake surface), water temperatures (at lake surface), and lake surface areas for the 1-year period of study. The integration assumed an instantaneous response of volatile selenium flux to changes in wind velocity and water temperature. The measured parameter values are shown for the period of study in [Figure 17a](#).

The volatile Se concentrations were discretely sampled and were temporally and spatially variable (areally and with depth). Flux estimates were based on volatile Se concentrations at depths of 0.2 to 0.5 m from the surface. Although these data are limited, they indicate decreased volatile Se concentration during winter ([Figure 17b](#)), and so were fitted using a sinusoidal function shown in [Figure 17b](#), according to the following equation:

$$C_{water}^{VSe} = 10^{\{A+B*\sin[(t-C)(D\pi)]\}} \text{ (ng Se/L)}$$

where A,B,C, and D are constants.

The concentration values span nearly two orders of magnitude; therefore the geometric mean is the better descriptor of the data than the arithmetic mean. The geometric mean (μ_g) is the n^{th} root of the product of n values, as follows:

$$\mu_g = \sqrt[n]{x_1 \cdot x_2 \cdot \dots \cdot x_n}$$

The geometric standard deviation (σ_g) is determined from the geometric mean as follows:

$$\sigma_g = \exp\left(\sqrt{\frac{\sum_{i=1}^n (\ln X_i - \ln \mu_g)^2}{n}}\right)$$

The geometric standard deviation is the ratio of the geometric mean to the 84th percentile (or inverse ratio to the 16th percentile) of the distribution of values, thereby describing 68% of the data (1st standard deviation).

The constants A through D were adjusted to yield the geometric mean (0.999 ng/L) and the geometric standard deviation (5.9) of the data for the period where volatile Se concentrations were actually measured (measurements were not taken between December 15th, 2006 and April 15th, 2007, due to logistical reasons). The corresponding values of the constants are shown in the equation below.

During integration, the following data frequencies were used for the lake area, temperature, and wind data: daily average for lake area, weekly average for water temperature and 1.5-hour intervals for wind speed. The cumulative integrated flux is shown as a function of time in Figure 17c.

Integration of the volatile Se flux yielded 2108 Kg of volatile Se lost to the atmosphere in 1 year.

3.2.4.1 Propagation of error in the calculation of the volatile Se flux

To determine error associated with the integrated flux, the estimated error for each parameter required to estimate flux was propagated. The individual errors were associated with near-surface water temperature, wind velocity, and volatile Se concentration (Table 6c), as described below.

The near-surface water temperature was incorporated into the Schmidt number shown below:

$$Sc_{DMeS}^{sea\ water}(T) = 2674.0 - 147.12T + 3.726T^2 - 0.038T^3$$

The error for this polynomial function was calculated using the derivative of the function, where:

$$\Delta Sc_{DMeS}^{sea\ water}(T) = 147.12\Delta T + 3.726 * 2\Delta T * T + 0.038 * 3\Delta T * T^2$$

where ΔSc is the error for the Sc number, ΔT is the error associated with measurement of the near-surface water temperature (± 0.5 °C).

The wind velocity (u_{10}) was incorporated into the air/water transfer velocity (k_w), shown below:

$$k_w(cm/h) = \left(\frac{Sc(T)}{600} \right)^{-1/2} (2 + 0.24u_{10}^2) \text{ for } u_{10} > 5 \text{ m/s}$$

$$k_w (cm/h) = \left(\frac{Sc(T)}{600} \right)^{-2/3} (2 + 0.24u_{10}^2) \text{ for } u_{10} \leq 5 \text{ m/s}$$

The error propagation for these functions can be calculated as follows:

for $u_{10} > 5 \text{ m/s}$

$$\Delta k_w (cm/h) = \left(\frac{2}{600} \right)^{-1/2} * \frac{\Delta Sc}{2 * Sc^{3/2}} + \left(\frac{0.24}{600} \right)^{-1/2} * \left(\frac{\Delta Sc}{2 * Sc} + \frac{2 * \Delta u_{10}}{u_{10}} \right) * Sc^{-1/2} * u_{10}^2$$

for $u_{10} \leq 5 \text{ m/s}$

$$\Delta k_w (cm/h) = \left(\frac{2}{600} \right)^{-2/3} * \frac{2 * \Delta Sc}{3 * Sc^{5/3}} + \left(\frac{0.24}{600} \right)^{-2/3} * \left(\frac{2 * \Delta Sc}{3 * Sc} + \frac{2 * \Delta u_{10}}{u_{10}} \right) * Sc^{-2/3} * u_{10}^2$$

where Δu_{10} is the error associated to wind velocity ($\pm 2.5 \text{ m/s}$) and Δk_w is the calculated error for the air/water transfer velocity.

The concentration of volatile Se (C_{water}^{VSe}) was incorporated into the expression for volatile Se flux to the atmosphere as shown below:

$$\text{Flux} = ak_w (C_{water}^{VSe}) * \text{Area}$$

where Area is the area of the South Arm of the Great Salt Lake.

The error associated with the volatile Se flux can therefore be determined as follows:

$$\Delta \text{Flux} = \text{Flux} * \left(\frac{\Delta k_w}{k_w} + \frac{\Delta (C_{water}^{VSe})}{(C_{water}^{VSe})} + \frac{\Delta \text{Area}}{\text{Area}} \right)$$

where $\Delta C_{water}^{VSe,eq}$ is the error associated with volatile Se concentration (factor of 5.9) and ΔArea is the error due to the variation in the lake area (± 427 acres per 0.1 stage inaccuracy).

The estimated error associated with k_w is approximately 100%, whereas estimated ΔArea was only a factor of 1E-3 relative to Area. By far the largest contributor to ΔFlux is ΔC_{water}^{VSe} for which the geometric standard deviation is 5.9.

The value of ΔFlux is therefore approximately 5.9, which is expressed as a geometric standard deviation. Hence, the expected 86th percentile value is $2108 \times 5.9 = 12,437$ Kg Se/yr, and the 16th percentile value is $2108 / 5.9 = 357.3$ Kg Se/yr. This large range in potential annual volatile Se flux results from the spatial and temporal variability of measured volatile Se concentration, as described above. It should be noted that the variability of the measured volatile Se concentration is not due solely to measurement error, as demonstrated by the significant correspondence between estimated and measured volatile Se fluxes, as described above.

3.3 Sedimentation fluxes

3.3.1 Downward sedimentation flux

The mass of sediment that accumulated in the traps over the period of deployment represents the downward sedimentation flux at that location over the period of deployment.

Sedimentation fluxes showed significant spatial variations (Figure 18 a-c and Table 7a). The sediment trap at shallow site (2267) yielded an average downward sediment flux of $2.95 \text{ g/cm}^2/\text{yr}$ for the period 03/23/06 to 06/26/07, which is an order of magnitude higher than any of the other average sediment fluxes measured during that period. The next-highest apparent sedimentation rates occurred at the two deep sites (2565 & 3510, Tables 7b & 7d), which were 0.53 and $0.35 \text{ g/cm}^2/\text{yr}$, respectively. The shallow sediment traps at sites 2565 and 3510 (Tables 7c & 7e) yielded very low downward sedimentation rates (0.035 and $0.068 \text{ g/cm}^2/\text{yr}$) that were approximately an order of magnitude below those of the corresponding deep traps.

The high sedimentation rates at shallow site (2267) correspond to its location in a relatively narrow channel between the Promontory Point and Fremont Island near the outlet of the Bear River. The observed peak sedimentation rate in spring corresponds to peak discharge from the Bear River.

The high sedimentation rates in the deep traps relative to the shallow traps at Sites 2565 and 3510 likely reflect re-suspension of sediment from the lake bottom, since it is unlikely that it represents increased sediment generation at intermediate depths. Had the material in the deep traps originated from shallower water, it would have also been collected in the shallow traps. This observation indicates significant re-suspension of lake-bottom sediment. The topic of re-suspension will be further described below.

In terms of temporal variation, all sites showed higher sedimentation rates in spring and early summer relative to late summer and fall (Figure 18 a-c and Table 7a).

The average Se downward fluxes mirror the spatial trends in downward sediment fluxes (Figure 18 and Table 7), where the average downward Se flux at shallow site 2267 ($1.44 \times 10^{-6} \text{ g Se/cm}^2/\text{yr}$) was one to two orders of magnitude larger than those at the deep sites (2565 & 3510, Tables 7b & 7d), which were 1.53×10^{-7} and $3.88 \times 10^{-8} \text{ g Se/cm}^2/\text{yr}$, respectively. The downward Se flux obtained at the shallow sediment traps at sites 3510 and 2565 yielded $3.18 \times 10^{-8} \text{ g Se/cm}^2/\text{yr}$ and $4.30 \times 10^{-8} \text{ g Se/cm}^2/\text{yr}$ (Tables 7e & 7c).

Regarding temporal variations, peak downward Se fluxes did not correspond to peak sedimentation fluxes (Figure 18), and did not show an apparent correspondence to season. However, the limited data would not be expected to yield a clear trend.

Collected sediment included mineral particles and organic material (e.g. phyto- and zooplankton, and brine shrimp). Based on visual inspection, mineral particles dominated the matrix at site 2267, whereas accumulated sediments at the other sites appeared to have mostly organic material. A notable exception occurred at site 2565 in April, 2006 when the matrix was dominated by mineral particles and the sedimentation flux was relatively high.

The downward sedimentation rates will be compared to net sedimentation rates below.

3.4 Permanent sedimentation or net sedimentation

3.4.1 Mass accumulation rates

Mass accumulation rates (MAR) were determined from ^{210}Pb and ^{226}Ra activity changes with depth in the sediment cores. Figure 19 presents a ^{226}Ra profile for site 3510, which is relatively constant in the core profile, whereas the total ^{210}Pb profile decreases with depth. Figure 20 shows the corresponding unsupported ^{210}Pb (^{210}Pb minus ^{226}Ra) profile for site 3510, which decreases exponentially with depth (cumulative sediment mass). This profile was used to calculate the net sedimentation rate as well as the date of the sediment profile.

The slope of the linear regression of Figure 20 determines the MAR. As an example, the permanent sedimentation rate for site 3510 was calculated to be $0.043 \text{ g/cm}^2/\text{yr}$. The MARs in the cores ranged from 0.010 to $0.049 \text{ g/cm}^2/\text{yr}$ with an average of $0.032 \text{ g/cm}^2/\text{yr}$ and two failing to yield sufficient ^{210}Pb activity for use in MAR estimation.

Sediment chronologies are shown as a function of depth for site 3510 in Figure 21a. The zone of near-constant ^{210}Pb activity between 0 and 3 cm may reflect a period of increased accumulation or mixing of the sediment due to physical processes, such as episodic re-suspension and re-deposition. Re-suspension is confirmed by the presence of ^7Be at 2 cm depth in the sediment (Figure 21b), indicating that all of the sediment in this interval was exposed to the water column within the past year.

Since the half-life of ^{137}Cs is 26 years, it can be used to confirm the dates obtained with unsupported ^{210}Pb . However, in this case the two methods disagreed. Figure 22 shows poor agreement between unsupported ^{210}Pb and ^{137}Cs , consistent with ^{137}Cs remobilization via desorption of ^{137}Cs from clays by cation exchange for ammonium ions produced during diagenesis. Subsequent diffusion of dissolved ^{137}Cs results in deeper penetration of the radionuclide, and upward migration of the activity maximum (Anderson et al., 1987), which is demonstrated in Figure 22.

In core samples from sites 2267 and 2565, the unsupported ^{210}Pb activities were too low to estimate MAR (Figures 23 & 24). In core 2267, unsupported ^{210}Pb was detected in the upper-most (0-2 cm) interval; whereas no measurable unsupported ^{210}Pb was observed in core 2565. The ^{210}Pb data may be indicative of very low sediment accumulation rates ($< 2 \text{ cm}/100 \text{ years}$ at 2267; and likely much lower at 2565). ^{137}Cs was undetectable by 8 and 6 cm in depth in cores 2267 and 2565, respectively (Figures 25 & 26). The greater depth of measurable ^{137}Cs compared to unsupported ^{210}Pb in

these cores is consistent with diagenetic remobilization of ^{137}Cs . ^7Be was detected in the surface interval (0-2 cm) in cores 2267 and 2565, suggesting some resuspension of this interval occurred during the past year. However, the much lower ^7Be activities in these cores relative to core 3510 indicate that resuspension occurs to a much lesser extent in these cores relative to core 3510.

3.4.2 Downward sedimentation vs. net sedimentation

A representative downward sedimentation flux from the shallow sediment traps at sites 2565 and 3510 can be considered to be representative of the main body of the Great Salt Lake. Representative sedimentation fluxes cannot be obtained from site 2267 due to its proximity to the Bear River. Nor can such a flux be obtained from the deep sediment traps at sites 2565 and 3510, due to the influence of re-suspension. The average sedimentation rate for these two shallow sediment traps is $0.016 \text{ g/cm}^2/\text{yr}$. This value is lower than the net sedimentation rate from the core at site 3510 ($0.043 \text{ g/cm}^2/\text{yr}$), indicating that the net sedimentation rate does not reflect through-fall from the surface. This discrepancy indicates that re-suspension and lateral transport of newly deposited sediment to permanent deposition zones is significant, in agreement with the ^7Be results.

Regarding downward Se sedimentation rate, the single significant value for the shallow sediment trap at site 3510 was $1.19 \times 10^{-8} \text{ g Se/cm}^2/\text{yr}$. This value is smaller than the net Se sedimentation rate from the core at site 3510 ($4.2 \times 10^{-8} \text{ g Se/cm}^2/\text{yr}$). Based on relative overall sedimentation rates, one might have expected the downward Se sedimentation rate to exceed the net Se sedimentation rate at site 3510 (reflecting re-suspension). However, lateral redistribution of Se is expected to occur as a result of re-suspension in the deep brine layer. Recall that Se accumulation in the deep traps at site 3510 was $1.4 \times 10^{-8} \text{ g Se/cm}^2/\text{yr}$, which matches the order of the net Se sedimentation rate ($4.2 \times 10^{-8} \text{ g Se/cm}^2/\text{yr}$).

3.4.3 Estimation of Se removal by sedimentation

Results of shallow core sedimentation rates overlain on Holocene thickness contours developed by Dr. David Dinter (University of Utah) are shown on the map in [Figure 27a](#). The geophysical measurements used in the development of these contours are described in Colman et al. (2002). The seven shallow cores that showed negligible ^{210}Pb activity are interpreted to indicate very low sedimentation rates at these locations (DD-A, DD-D, DD-G, DD-H, DD-K, DD-O, DD-S). In general, Holocene thickness and sedimentation rates were high along the fault slightly west of the shore of western Antelope Island. East of this line, Holocene thickness decreased dramatically. West of the fault, the sedimentation rates and Holocene thicknesses fell more slowly, but continued to decline to the western shore of the south arm of the GSL (Dinter, 2007). The contours bounding the 5 zones developed to reflect different sedimentation rates are shown in [Figure 27b](#). The qualitative “very low” sedimentation zone had the largest area, with areas decreasing with each increasing step in sedimentation rate.

The net Se sedimentation rate was determined by multiplying the average Se concentration in the 5-10 cm interval (which showed relatively constant values, [Figure 27c](#)), by the net sedimentation rate. The average selenium concentrations below 5 cm in the 8 cores are shown in [Table 8](#). The concentrations ranged from 0.05 to 1.96 ug/g with an average of 0.95 ug/g. With the exception of the “very high” sedimentation zone, the average selenium concentration in each sedimentation zone was determined by averaging the below-5-cm selenium concentrations within the zone. The Holocene thickness-based “very high” sedimentation zone did not contain any cores, and so was assigned a selenium concentration based on that in the “high” sedimentation zone, as described below.

Average mass accumulation rate (MAR) in each zone was determined by interpretation of the MAR results from the deep cores ([Table 9](#)). MARs in the “medium” and “high” zones were found by averaging the cores that fell within them. The MAR in the “low” zone contained three cores with sufficient ^{210}Pb activity to estimate MARs; however, core DD-I was not taken into consideration because the MAR value from the long core (0.049 g/cm²/yr) and linear sedimentation rate from the short core (95 cm/yr) indicate that it is an outlier and processes may be occurring in that location that are not representative of the entire “low” sedimentation area. It is possible that this outlier reflects anomalous sedimentation influences, for example, from causeway construction activities. The MAR for the “low” sedimentation zone was, therefore, calculated by averaging the two remaining cores with sufficient ^{210}Pb activity (DD-Q and 3510) with a sedimentation rate of zero for core 2267 (based on insufficient ^{210}Pb indicating very low sedimentation rate) – yielding an average MAR of 0.018 g/cm²/yr. The “very low” sedimentation zone did not contain any cores with sufficient ^{210}Pb activity to estimate a MAR. Therefore, the representative MAR for this zone was estimated to be a factor of 2 below the value for the “low” sedimentation zone. The MAR for the “very high” sedimentation zone was estimated as 0.05 g/cm²/yr, 25% higher than the “high” zone value.

Due to the method of analysis of ^{210}Pb decay (use of the slope of the trendline of the natural logarithm of unsupported ^{210}Pb), standard deviation errors could not be propagated through to the final MAR values for each core. However, to estimate possible error in MAR values, 1 standard deviation was added and subtracted to the unsupported ^{210}Pb value in each 1-cm increment of the cores. Following the CF-CS method described in section 3.3.2.1 above, the MAR for +1 and -1 standard deviation was calculated. As an example, in core DD-C, both standard deviations yielded MAR values above that of the originally calculated MAR ([Figure 27d](#)), although both were within a factor of 2. As another example, in core DD-I, the MAR values from the +1 and -1 slopes were 0.015 and 0.055 respectively as compared to the original MAR of 0.049 ([Figure 27e](#)). The factor of two range in MAR obtained from core DD-I, and the much lower range obtained in core DD-C, bounds the ranges observed in the other cores using this approach. This leads us to conclude that using a geometric standard deviation of 2 (multiplying and dividing each MAR result by 2) encompasses the MAR values and is appropriate for error estimation.

William P. Johson 11/1/07 5:32 AM

Comentario: Although there may be some diagenetic effects on the selenium deposited in the sediments, we also have to consider the possibility that the last 50 years of sediment flux to GSL has had higher selenium contents.

The low selenium concentrations in the upper core samples (associated with the high organic flocculent) are being diluted significantly by salt from the pore water. These concentration values need to be corrected by subtracting out the essentially 0 ppm Se contribution by the solid phase salt precipitate that is being measured as part of the mass during analysis. (Wade Oliver or Ximena Diaz)

Table 10 shows the selenium concentration, MAR, area, and calculated mass of Se removed annually within each sedimentation zone. Table 11 shows the range of Se removed annually within each sedimentation zone based on the MAR error estimated above. Results indicate that about 248 kg of Se are permanently removed from the GSL by sedimentation each year with a range of 124 to 496 kg/yr.

3.4.4 Sediment trace element analysis

Trace element concentrations as a function of depth at site 3510, show maxima at a depth of several cm (Figure 28). In contrast, trace elements concentrations at the two other sites analyzed show maximum values near the surface (Figures 29 & 30). The trace elements that show increased concentrations near the sediment surface are those expected from mining activities and urban development. These increases in the top 10 cm correspond to development of the basin (past 100 years), according to the chronology from site 3510. However, diagenetic changes may have influenced the concentration-depth profiles such that historical trends may not be accurately recorded (Callendar, 2000).

William P. Johnson 10/28/07 12:50 PM
Comentario: Show as linear instead of log? Harry says no. Save for after Panel Review

3.5 Re-suspension – Re-solubilization

3.5.1 Temperature stratification

3.5.1.1 Seasonal trends

Temperature in the water column of the Great Salt Lake varies seasonally with highest temperatures observed in summer and lowest in the winter (Figures 31a & b). At sites 2565 and 3510 (Figure 1) the water column is stratified due to the presence of the deep brine layer. During the summer the deep brine layer was cooler than shallow brine layer and reversed in the winter when the deep brine layer was warmer than the shallow brine layer (Figures 31a & b).

Periodic events punctuate the record of temperature stratification when temperatures equilibrate to a single value across the measured depth of the water column (Figure 31c). At least eight of these equilibration events occurred during the 6-month period of observation from June to December 2006. From January through June 2007 at least six temperature equilibration events were recorded. Five of the events at site 2565 during that 6-month period occurred within a ten day period during the month of April (Figure 31c). Equilibration events ranged in duration from 12 to 24 hours. All significant equilibration events were associated with wind speeds greater than about 30 mph (e.g., Figures 32 a & b), signaling that wind speed drove the equilibration process. The wind direction may also influence the temperature equilibration process as indicated by the muted response at site 3510 relative to site 2565 to the increase in wind speed on October 16th. A change in wind direction from 250 to 360 (or zero) degrees yielded a strong temperature equilibration response at site 3510 (Figure 32b), indicating that this northerly wind yielded great influence at site 3510 relative to the westerly wind. The different responses of the two sites are likely related to their being located in two

different sub-basins in the south arm of the Great Salt Lake, as shown by the bathymetric map (Figure 1).

3.5.1.2 Lake Mixing

3.5.1.3 Langmuir circulations

Temperature equilibration events in the water column may represent genuine mixing of the deep and shallow brine layers. One means of achieving this vertical mixing is Langmuir circulation (Wetzel, 2001), which involves helical advection within the water column in response to wind shear. The diagnostic feature of Langmuir circulation is longitudinal streaks oriented with the dominant wind direction.

At wind velocities of 2-7 m/s or greater, streaks of aerated water and floating materials are observed at the water surface (Wetzel, 2001). The spacing between streaks is proportional to the depth over which helical circulation occurs (mixing depth). Assuming symmetric helical cells, mixing depth is equal to half of the distance between adjacent streaks.

3.5.2 Seiche

An internal seiche may result from the wind loading of water in response to atmospheric pressure changes. The loading of water forces the displacement of water at depth, producing an internal wave that may be transmitted across the water body. In a stratified system, deeper layers of the water column may be temporarily displaced in the zone of the internal wave.

3.5.3 Mechanism of temperature equilibration events

Langmuir circulation is a candidate mechanism to drive actual mixing of the water column. The maximum depth of the water column in the south arm of the Great Salt Lake is about 9 m. In order to mix the water column to this depth, the spacing between Langmuir circulation-produced surface streaks would need to be 18 m. Streaks associated with Langmuir circulations have been observed on the Great Salt Lake in this study and have been previously documented (Stommel, 1951). Although to our knowledge no quantitative measurements of streak spacing have been performed on the Great Salt Lake, observed streak spacing was qualitatively consistent with magnitude needed to mix the deep brine layer. Such mixing depths have been observed in lakes of much smaller areal extent. Maximum mixing depth observed at Lake George, NY was between 10 and 15 m (Langmuir, 1938).

If the temperature equilibration events represent true mixing of the entire water column, one would expect the final temperature to reflect mixing of the initially stratified water column temperatures. The final temperature calculated using the thermal mixing approach for an equilibration event on June 14, 2006, yields 19.7°C. The measured

temperature during this event remained near 21°C (Figure 32a), suggesting that actual mixing of the entire water column did not occur.

The nature of the temperature equilibration events, in terms of time passed during equilibration and re-stratification of temperature; can also be used to deduce the mechanism. The response of temperature was rapid, with equilibration often occurring over periods less than an hour. For example, on June 14, 2006 at site 2565, the temperature of the deepest thermistor increased from 17°C to 21°C (temperature of shallow thermistors) over the 70-minute period from 02:27 to 03:39 (Figure 32a). The termination of temperature equilibration and return to stratified temperature conditions also occurred over short time periods (Figures 32 a & b).

Another clue to the mechanism of temperature equilibration is provided by the observation that equilibrated temperature was always that of the shallow brine layer regardless of which layer (shallow or deep brine) was warmer. This observation indicates that temperature equilibration occurred via displacement of the deep brine layer, which is an effect that is consistent with a seiche-driven internal wave. Historical evidence of surface seiche activity has been documented on the south arm of the Great Salt Lake (Lin, 1977). Increase in the lake level at the north end of the lake (Promontory Point) corresponds with a decrease in lake level at the south end of the lake (Silver Sands) following a strong wind event (Figure 33a). Ranges in the magnitude of the lake level change associated with a seiche event vary with distance across the lake (Figure 33b).

Evidence of surface seiche activity on the lake was recorded at the USGS Saltair Gauge for both temperature equilibration events discussed above. Gauge elevation increased from 0.5 m to 1 m after a wind event, and elevation oscillated after initial surge about the initial lake elevation value (Figures 31c, 34a and 34b). The duration of the period over which lake elevation oscillated significantly was similar to the duration of the period over which temperatures responded and periodically equilibrated to the shallow brine temperature. Furthermore, the timing of individual complete temperature equilibration events corresponded to peaks in the lake elevation oscillations, demonstrating a strong relationship between lake elevation oscillation and temperature equilibration. This indicates that loading of water at the surface of the lake induced an internal seiche that displaced the deep brine layer as it passed.

Assuming that the period of an internal seiche corresponds to the period of temperature equilibration, a comparison can be made between the estimated period of an internal seiche and the period of temperature equilibration. The observed duration of temperature equilibration events was sometimes long; for example, the June 14, 2006 equilibration event included a 24-hour period of complete equilibration. This long period of equilibration is similar to what is predicted by the expression for the period of a uninodal internal seiche, which is 25.6 hours for a 40-Km length corresponding to the basin south of the submerged ridge of the Carrington fault. Obviously the actual seiche may not be uninodal, and so the estimated period is based only on a simplified approximation. Another aspect of the temperature equilibration events that is suggestive transmission of an internal wave is the oscillation between complete equilibration and partial stratification that was observed during the temperature

equilibration events discussed above. For example, during October 17 and 18th, 2006, site 3510 showed several of these oscillations that corresponded approximately to a 6-hour period. This period was far smaller than the estimated period of an idealized seiche; however, the oscillatory nature of these events was consistent with the transmission of an internal wave.

3.5.4 Batch equilibration tests

Total Se concentrations in bed sediment samples were analyzed at LET and the University of Utah, and results showed good correlation (Figure 35a). The average Se concentration for the 30 samples analyzed was 1.0±0.30 mg/Kg (LET) and 1.24±0.22 mg/Kg (University of Utah).

Following 24 hours of contact between the bed sediments and the shallow brine water, the resultant Se concentration in water varied among the sediment samples, with the highest concentrations found in samples with air headspace.

Percent Se solubilized (of extractable) varied spatially with no discernable pattern (Figure 35b). The average percent Se solubilized in the samples with nitrogen gas headspace was 1.18±0.68 %, whereas the average percent Se solubilized in the samples with air headspace was 1.16±1.36 %. The maximum percent solubilized was from site GS 11 composite with air headspace at 6.07% (Figure 36).

Solubilization of Se into the water column due to equilibration of anoxic sediment with shallow brine layer may occur periodically, in response to wave-induced sediment re-suspension and seiche-driven displacement of the deep brine layer. The significance of these events to Se concentration is demonstrated by an example scenario based on observed sediment re-suspension into the sediment traps. Since approximately 1 g of sediment is periodically re-suspended into the sediment traps (3.6 cm radius), a 3.6-cm column of water can be expected to equilibrate with 1 g of sediment. Assuming that the equilibrated column of water is 4 m in height, the resulting additional Se concentration from equilibration with anoxic sediment is:

$$Se_{add} \left(\frac{ig_{solubilized}}{L} \right) = \left(\frac{1.31 ig_{extracted}}{g_{sed}} \right) \left(\frac{0.1476 ig_{solubilized}}{2.4340 ig_{extracted}} \right) \left(\frac{1 g}{\pi (0.036 m)^2 (4 m)} \right) \left(\frac{m^3}{1000 L} \right)$$

$$Se_{add} = 0.0049 \frac{ig_{solubilized}}{L}$$

Where: Se_{add} is the additional Se concentration in the water column ($\mu\text{g/L}$); Se_{sed} is the concentration of Se in the sediment ($\mu\text{g/g}$); Se_{ratio} is the amount of Se solubilized in the batch test divided by the amount of Se extracted during sediment digestion ($\mu\text{g}/\mu\text{g}$); w is the weight of sediment in deep sediment trap (g); r is the internal radius of a sediment trap tube (m); and h is the height of the water column over which the Se from the sediment is mixed (m).

The resultant additional Se concentration from site GS 11 is 0.0049 µg/L, which is a negligible value compared to aqueous Se concentrations measured in the lake. Site GS 11 represents the greatest potential for additional concentration based on batch test measurements. The average additional Se concentration contribution for samples with either air or nitrogen headspace is 0.0009 µg/L. Reduction of the equilibrated water column length by a factor of 10 (0.4 m) would still yield negligible additional Se concentration. The contribution from re-suspension is therefore not likely to significantly increase the concentration of Se of the water column.

3.6 Mass balance

The total Se mass in the Great Salt Lake calculated for May 2006 was 4780 Kg. Of that, 3187 Kg (66.6%) was dissolved (< 0.45 µm) and 1596 Kg (33.4%) was bound to particulates (> 0.45 µm). In July 2007, the total Se mass in the lake was 7677 Kg, of which 6233 Kg (81.2%) was dissolved, and 1444 Kg (18.8%) was bound to particulates. These example values demonstrate that about 20% to 30% of Se mass in the water column of the Great Salt Lake was associated with particulates.

According to the loading report (Naftz et al., 2007), about 1,480 Kg Se/yr are introduced to the south arm of the Great Salt Lake annually (dissolved plus particulate). Given the present volume of the Great Salt Lake, a Se concentration of 15 µg/L would result from just 100 years of loading if Se were conservative. Clearly, given the ~10,000 year history of the lake, removal mechanisms (e.g., sedimentation, volatilization, and brine shrimp harvest) have influenced the observed concentration towards the present observed average concentration of 0.49 µg/L.

The brine shrimp industry removed 16.6 million pounds of cysts and Artemia biomass over the 2006-2007 season (Marden, 2007). A characteristic industry estimate is 23% dry yield for the commercial harvest (Marden, 2007). The range of average tissue selenium concentrations were 1.18 ug/g dw (Marden, 2007) to 5.7 ug/g dw (Conover, 2007). The resulting range in Se mass flux via the brine shrimp harvest is from 9.9 to 48 Kg/yr.

The fluxes of Se out of the south arm of the Great Salt Lake were estimated to be: 1) a permanent sedimentation flux of 248 Kg/year (arithmetic mean); 2) an integrated volatilization flux of 2108 Kg/yr (geometric mean); and, 3) Se flux via brine shrimp harvest of 28 Kg/yr in 2006-2007 (intermediate value from above). These loss fluxes total to 2384 Kg/yr. The mean volatile and mean permanent sedimentation Se fluxes are 10% and 89%, respectively, of the overall Se removal flux based on the above estimates (Figure 37). The loss flux (2384 Kg/yr) exceeds the estimated loading (1,480 Kg/yr). The flux estimation indicates that the annual Se losses balance the Se loads, with the largest loss mechanism being volatilization. The results demonstrate that sedimentation is a relatively minor mechanism of Se removal from the Great Salt Lake, and that most Se removal occurs via volatilization. The percentage distribution corresponding to the low and high values of the removal fluxes are also presented in Table 12 and Figure 37.

William P. Johson 11/1/07 5:59 AM

Comentario: We will add a paragraph about contribution from shrinkage of the deep brine layer (Kim Beisner).

William P. Johson 11/27/07 8:46 PM

Comentario: Need the full references for Marden and Conover's reports. CH2M, do you have these reports to share?

William P. Johson 11/27/07 8:21 PM

Comentario: Jeff suggests including the flux of Se removed via brine shrimp grazing by birds (e.g. 2.5 million grebes times #shrimp per grebe. Need report from Conover for this number.

As shown in Figure 7, and as described in the loading report (Naftz et al., 2007), the aqueous Se concentration in the Great Salt Lake increased by an amount ranging from 0.16 to 0.34 mg/L during the period of observation (May 2006 to July 2007). This was a surprise considering the apparent balance of load and removal fluxes described above. Assuming conservative behavior of Se, Naftz et al. (2007) calculated the existence of an unmeasured load of approximately 1350 Kg/yr (1500 Kg during the 15-month period of study).

The concentration trajectories of total Se (dissolved plus particulate) over the course of the study were explored by integrating the total Se concentration over time via the following mass balance:

$$[Se]_t = [Se]_{t-1} + \frac{[Se_{load} - Se_{volatilization} - Se_{permanent\ sedimentation} - Se_{brine\ shrimp\ harvesting}]}{Volume}$$

where $[Se]_t$ and $[Se]_{t-1}$ represent the total Se concentration in $\mu\text{g/L}$ for the present and previous time steps, respectively; Se_i (i = load or removal process) represents the mass flux (loading or removal) per unit time; and Volume represents the volume of the lake. The mass balance was determined from May 19, 2006 to August 1, 2007 using daily values of fluxes (loads and removal processes). The daily values for loads and volatilization were determined as described in Naftz et al. (2007) and this report, respectively; whereas the daily values for permanent sedimentation and brine shrimp harvest were determined by division of the annual values by 365. Daily values of surface area and volume of the Great Salt Lake, for the same period, were obtained from the USGS National Water Information System (<http://waterdata.usgs.gov/nwis>).

The trend in total Se concentration, without inclusion of removal processes (Figure 38), showed an increase during the time period of the investigation, with the final estimated total Se concentration ($0.64 \mu\text{g/L}$) nearly matching the measured value in July, 2007 ($0.75 \mu\text{g/L}$ = average of the four sites). Addition of the removal processes (volatilization, permanent sedimentation and brine shrimp harvesting), yielded decreases in the estimated total Se concentration during the time period of the investigation (Figure 38). For the mean fluxes of volatilization and permanent sedimentation, the final estimated total Se concentration was ($0.36 \mu\text{g/L}$), which was low (by about $0.4 \mu\text{g/L}$) relative to the measured value in July, 2007 (Figure 38). For the low fluxes of volatilization and permanent sedimentation, the final estimated total Se concentration was ($0.58 \mu\text{g/L}$) somewhat below (about $0.17 \mu\text{g/L}$) the measured value in July, 2007. These results suggest that the actual volatilization flux is in the low end of the spectrum of estimated values.

Potential source(s) of the unmeasured Se load that were previously described by Naftz et al. (2007) include: (1) submarine groundwater discharge; (2) wet and dry atmospheric deposition falling directly on the lake surface; (3) lake sediment pore water diffusion into the overlying water column; and (4) poorly characterized exchange with the north arm, as described in the report regarding Se loads to the Great Salt Lake.

For all measurements made during this flux study, the dissolved volatile Se concentrations increased with depth, demonstrating that the dissolved volatile Se flux was outward (to the atmosphere) for all measured periods. However, this observation does not preclude the possibility that the total Se concentration increased with depth, since the dissolved volatile Se concentration comprises only 0.1% of the total aqueous Se concentration. Furthermore, it is possible that the near-surface Se concentration gradient differs during precipitation events, which could not be measured due to logistical limitations.

Estimated values of atmospheric Se deposition for several global sites are presented in Table 13. A highly speculative literature-based estimate of dry deposition for the Great Salt Lake ($162.67 \mu\text{g}/\text{m}^2/\text{yr}$) was developed by averaging estimated dry deposition at the Great Lakes and Chesapeake Bay. This estimated dry deposition flux yields an estimated atmospheric load of 300 Kg/yr.

When atmospheric deposition (300 Kg/yr) was included in the trajectory simulations using the low values of the estimated volatilization and sedimentation fluxes, the final estimated Se concentration was $0.61 \mu\text{g}/\text{L}$ (Figure 39), which was approximately $0.14 \mu\text{g}/\text{L}$ below the measured value. This suggests that the observed trajectories can be explained by a combination of unmeasured loads and removal fluxes that correspond to the low end of the estimated range.

3.7 Variability

The mass balance section necessarily simplified the characteristics of the Great Salt Lake in order to allow the development of a simple mass balance. In reality, the Great Salt Lake is neither vertically nor areally homogenous.

Data presented above speak to the vertical heterogeneity, that is, the density stratification of the lake. The denser Deep Brine Layer of the Great Salt Lake is anoxic, and is therefore geochemically distinct from the oxic Shallow Brine Layer. The dynamics of the Deep Brine Layer, and its influence on Se, as well as other trace metal and metalloid cycling, needs to be better understood. The evolution of the Deep Brine Layer from its origin at the north arm to its apparent assimilation via mixing at the south end of the lake needs to be investigated in order to understand the time and space scales over which anoxia occurs, and over which oxidized trace metals and metalloids are reduced to other forms. With this understanding, it may be possible to design strategies to mitigate negative influences of the Deep Brine Layer on the cycling of particular trace metals (e.g. Hg).

The measured volatile Se concentrations in the water column demonstrate vertical variation, where a distinct increase in volatile Se concentration with depth was observed in the Shallow Brine Layer (Table 5 and Figure 15a); whereas no such trend was observed in the Deep Brine Layer (Table 5 and Figure 15b). This trend may implicate phytoplankton as the generators of volatile Se. The trend seems to be more clearly established for the shallow sites (2267 and 2767), possibly suggesting the bioherms as

an important source of volatile Se, or possibly suggesting the importance of proximity to labile carbon sources such as the Bear and Weber rivers and Farmington Bay.

The measured downward sedimentation fluxes (Table 7 and Figure 18) demonstrate that areal variability exists with respect to downward sedimentation in the Great Salt Lake. Site 2267 in the Bear River Strait showed downward sedimentation values that were one to two orders of magnitude higher than sites 3510 and 2565. Temporal variability is also evident with orders of magnitude higher downward sedimentation fluxes during spring and summer relative to fall and winter. The higher downward sedimentation flux in the Bear River Strait is likely due to its proximity to the Bear River, which is the presumed source of the corresponding particulates.

As shown in the Naftz et al. (2007) report, the total Se concentration increased over the course of the study. This increase was also observed in the dissolved ($< 0.45 \mu\text{m}$) concentrations, with an average increase of $0.35 \mu\text{g/L}$ (Figure 40a). Areal variability is demonstrated in this data, where sites 2267 and 2767 show greater increases in Se concentration (dissolved and total) relative to sites 2565 and 3510. The latter two sites have deep brine layers, which could potentially act as an Se sink; whereas the former two sites are located nearest to major load points (Bear and Weber Rivers, and Farmington Bay causeway), which may locally enhance Se loading. Notably, particulate-associated Se concentration trajectories did not show an increase over the course of the study (Figure 40b).

Although suspension of consideration of the above-described variability in the south arm of the Great Salt Lake was useful for ease of implementation of the mass balance, the observed variability provides clues to important processes that control the cycling of Se in the system, and warrant further investigation. Furthermore, the period of observation was merely 15 months and fortunately coincided with a transition to reduced runoff. However, a more complete understanding of the system will be achieved with continued observation, including transition to periods of increased runoff.

References

Amouroux, D. (1995) Ph.D. Thesis, University of Bordeaux I, Bordeaux, France.

Amouroux, D., Tessier, E. and Donard, O.F.X. (2000) Volatilization of organotin compounds from estuarine and coastal environments, *Environ. Sci. Technol.* **34**: 988-995

Amouroux, D. and Donard, O.F.X. (1996) Maritime emission of selenium to the atmosphere in eastern Mediterranean seas, *Geophysical Research Letters*, **23**(14): 1777-1780

Anderson, R.A., Schiff, S.L., and Hesslein, R.H. (1987). Determining sediment accumulation and mixing rates using ^{210}Pb , ^{137}Cs and other tracers: Problems due to postdepositional mobility or coring artifacts. *Canadian Journal of Fisheries and Aquatic Sciences*, **44**:231-250.

Appleby, P.G. and Oldfield, F. (1992). Application of ^{210}Pb to sedimentation studies. Chapter 21. IN: Ivanovich, M., and Harmon, R.S., Ed., Uranium-series Disequilibrium: Application to Earth, Marine, and Environmental Sciences, Second edition. Clarendon Press, Oxford, pp. 731-778

Atkinson, R., Aschmann, S.A., Hasegawa, D., Thompson-Eagle, E.T. and Frankenberger, W.T., Jr. (1990). Kinetics of the atmospherically important reactions of dimethyl selenide, *Environmental Science and Technology*, **24**:1326-1332

Baker J.E., Burdige D., Church, T.M., Cutter G., Dickhut, R.M., Leister, D.L., Ondov, J.M. and Scudlark J.R. (1994) The Chesapeake Bay Atmospheric Deposition Study. Phase II Final Report, July 1990-December 1991,

Baskin, R.L. (2005) Calculation of area and volume for the south part of the Great Salt Lake, Utah. U.S. Department of Interior, U.S. Geological Survey, Open-File Report 2005 - 1327

Byron, E.R. and Ohlendorf H.M. (2006) Selenium flux and speciation from lake sediment as influenced by quality of overlying water: evaluating restoration alternatives for the Salton Sea. Abstracts with Programs AGU Conference, San Francisco.

Callendar E. (2000) Geochemical effects of rapid sedimentation in aquatic systems: minimal diagenesis and the preservation of historical metal signatures, *J. of Paleolimnology* **23**: 243–260.

Card, T., C.E. Schmidt, J. Witherspoon, L. Koe, "Theoretical and Practical Considerations in the Use of Wind Tunnel for Odor Emission Measurement," Paper No. 42654, 95th Annual Meeting of the Air and Waste Management Association, Baltimore, MD, June, 2002.

- Clark, J.F., Schlosser, P., Simpson, H.J., Stute, M., Wanninkhof, R. and Ho, D.T. (1995). Relationship between the gas transfer velocities and wind speeds in the tidal Hudson River determined by the dual tracer technique. IN: Air-water gas transfer, Jähne, B. and Monahan E.C., Eds., AEON Verlag, Hanau, Germany, pp. 785-800
- Cole, G.A. (1983) Textbook of limnology. 3rd ed. Mosby, St. Louis.
- Colman S.M., K.R. Kelts, D.A. Dinter (2002) Depositional history and neotectonics in Great Salt Lake, Utah, from high-resolution seismic tomography. *Sedimentary Geology*, **148**: 61-78.
- Crosman, E. and Horel, J. (2006) Remote sensing of the temperature of the Great Salt Lake, submitted to *Journal of Geophysical Research - Oceans*.
- Cutter, G.A. and Cutter, L.S. (1998) Metalloids in the high latitude North Atlantic Ocean: Sources and internal cycling. *Marine Chemistry*, 61:25-36
- Cutter, G.A. and Cutter, L.S. (2001) Source and cycling of selenium in the western and equatorial Atlantic Ocean. *Deep-Sea Research II*, 48:2917-2931
- Cutshall, N.H., Larsen, I.L., and Olsen, C.R. (1983). Direct analysis of ²¹⁰Pb in sediment samples: self-absorption corrections. *Nuc. Inst. and Methods*, **306**:309-312.
- Dinter, David, Lecturer, Department of Geology & Geophysics, University of Utah. Suggested Core Sample Locations in the Great Salt Lake Based on Long-term Holocene Depositional Rates Estimated from Chirp and Geopulse Seismic Reflection Profiles. May 9, 2007.
- EPA (2007) Multi-Media, Multi-Concentration, Inorganic Analytical Service for Superfund (ILM05.3), EPA Publication 540-FS-07-004
- Fuller, C.C., vanGeen, A., Baskaran, M., and Anima, R. (1999). Sediment chronology in San Francisco Bay defined by ²¹⁰Pb, ²³⁴Th, ¹³⁷Cs, and ^{239,240}Pu. *Marine Chemistry*, **64**:7-27.
- Guo L., Jury W.A., Frankenberger W.T., 2000, Measurement of the Henry's constant of dimethyl selenide as a function of temperature, *Journal of Environmental Quality* **29** (5): 1715-1717.
- Horel, J. (2007) Personal communication, Meteorology Professor, University of Utah.
- Langmuir, I. (1938) Surface motion of water induced by wind. *Science*, **87**: 119-123.
- Lin, A. (1977) Final Report on Wind Tides of the Great Salt Lake, Submitted to Utah Geological and Mineralogical Survey.

Liss, P.S., and Merlivat, L. (1986) Air-sea gas exchange rates: Introduction and synthesis. IN: P. Buat-Ménard, Ed., The role of air-sea exchanges in geochemical cycling, D. Reidel Publishing Company, pp. 113-127

Livingstone, D.M. and Imboden, D.M. (1993) The non-linear influence of wind variability on gas transfer in lakes. *Tellus Ser. B*, **45**:275-295

Masscheleyn, P.H. and Patrick, W.H. (1993) Biogeochemical processes affecting selenium cycling in wetlands. *Environmental Toxicology and Chemistry*. **12**:2235-2243.

Marden, B. (2006) Personal communication

Naftz, D.L., Johnson, W.P., Freeman, M., Beisner, K. (2007) Estimation of selenium loads entering the South Arm of Great Salt Lake, Utah: Preliminary results.

Neumann, P.M., De Souza, M.P., Pickering, I.J. and Terry, N. (2003) Rapid microalgal metabolism of selenate to volatile dimethylselenide, *Plant, Cell and Environment*, **26**:897-905

Saltzman, E.S. and King, D.B. (1993) Experimental determination of the diffusion coefficient of dimethyl sulfide in water, *J. Geophys. Res.* **98**(C9):16481-16486

Schmidt, C.E., 2007, personal communication with the designer of the USEPA Flux Chamber,

Schwarzenbach, R.P., Gschwend, P.M. and Imboden, D.M. (2003) Environmental Organic Chemistry, 2nd. Ed., Wiley-Interscience, Hoboken, NJ, pp. 159-163, 887-921

Stommel, H. (1951) Streaks on natural water surfaces. *Weather*, **6**:72-74.

Sweet C.W., Weiss A. and Vermette, S.J. (1998) Atmospheric deposition of trace metals at three sites near the Great Lakes. *Water, Air and Soil Pollution*, 103:423-439

Tessier E, Amouroux, D. and Donard, O.F.X. (2003) Biogenic volatilization of trace elements from European Estuaries, Chapter 12. IN: Biogeochemistry of environmentally important trace elements, Cai, Y. and Braids, O.C. (Eds), American Chemical Society, Washington, pp. 151-165

Van Metre, P.C., Horowitz, A.J., Mahler, B.J., Foreman, W.T., Fuller, C.C., Burkhardt, M.R., Elrick, K.A., Furlong, E.T., Skrobialowski, S., Smith, J.J., Wilson, J.T., and Zaugg, S.D. (2006) The impact of hurricanes Katrina and Rita on the chemistry of bottom sediments in Lake Pontchartrain, Louisiana, USA. *Environmental Science and Technology*, **40**:6895-6902

Wetzel, R.G. (2001) Limnology. 3rd ed. Saunders, Philadelphia.

Wind Energy Department of Risoe National Laboratory and Det Norske Veritas: Guidelines for Design of Wind Turbines, Copenhagen (2001). ISBN 87-550-2870-5

TABLES

Table 1a. ICP-MS conditions for water sample analysis

Condition	Value
RF power (W)	1550
Plasma gas flowrate (L/min)	15.0
Hydrogen flowrate (mL/min)	5.0
Helium flowrate (mL/min)	6.5
Carrier flowrate (L/min)	0.73
Make-up gas (L/min)	0.21
Auxiliary gas (L/min)	1.0
Sample pump (rps)	0.1
Sample depth (mm)	8.0
Tuning solution:	
⁷ Li mean (cps)	30,000
⁸⁹ Y mean (cps)	29,000
²⁰⁵ Th mean (cps)	64,000
% RSD for each cps	< 3%
Sample nebulizer tubing:	
Material	Tygon
Internal diameter (mm)	1.02
Internal standard tubing:	
Material	Tygon
Internal diameter (mm)	0.91

Table 1b Great Salt Lake synthetic solution recipe

Salt	Concentration (mol/g_{solution})	Concentration g/L	Grams in 100mL milliQ W	Salt Purity	Salt brand
NaCl	1.99E-03	116.7884	11.6788	99.999%	Sigma- Aldrich
MgCl ₂	1.46E-04	13.9657	1.3966	99.99%	Sigma
MgSO ₄	3.73E-05	4.4874	0.4487	99.99+%	Aldrich
K ₂ SO ₄	3.21E-05	5.5877	0.5588	99.99%	Aldrich
CaSO ₄	4.88E-06	0.6306	0.0631	99.99+%	Aldrich

Table 1c. Quality control summary (EPA, 2007)

QC Operation	Frequency
Instrument Calibration	Daily or each time instrument is set up.
Initial Calibration Verification (ICV)	Following each instrument calibration for each wavelength or mass used.
Initial Calibration Blank (ICB)	Following each instrument calibration, immediately after the Initial Calibration Verification (ICV).
Continuing Calibration Verification (CCV)	For each wavelength or mass used, at a frequency of 10% or every two hours of a run, whichever is more frequent, and at the beginning and end of each run.
Continuing Calibration Blank (CCB)	10% or every two hours of a run, whichever is more frequent, and at the beginning and end of each run. Performed immediately after the last Continuing Calibration Verification (CCV).
CRQL Check Standard (CRI)	Every 20 analytical samples and at the beginning and end of each run, but not before the ICV. Performed before the Interference Check Sample.
Interference Check Sample (ICS)	For ICP-AES, every 20 analytical samples and at the beginning and end of each run, immediately after the CRI. For ICP-MS, at the beginning of the run.
Serial Dilution for ICP	For each matrix type or for each SDG, whichever is more frequent.
Preparation Blank	For each SDG or each sample preparation and analysis procedure per batch of prepared samples.
Laboratory Control Sample	For each SDG or each sample preparation and analysis procedure per batch of prepared samples, except aqueous mercury and cyanide.
Spike Sample	For each matrix type or for each SDG, whichever is more frequent.
Post Digestion/Distillation Spike	Each time Spike Sample Recovery is outside QC limits.
Duplicate Sample Analysis	For each matrix type or for each SDG, whichever is more frequent.
ICP-MS Tune	Prior to calibration.
Method Detection Limit Determination	Prior to contract, annually thereafter, and after major instrument maintenance.
Interelement Corrections	Prior to contract, quarterly thereafter, and after major instrument adjustment.
Linear Range Analysis	Prior to contract, and quarterly thereafter.

Table 2a. Total (RA) and dissolved (FA) selenium concentrations in water, site 2267.

Site	Sampling date	Depth (m)	FA (ppb)	RA (ppb)	
2267	26-May-06	0.2	0.311	0.404	
	26-May-06	4	0.341	0.524	
	19-Jun-06	0.2	0.267	0.311	
	19-Jun-06	4	0.278	0.405	
	28-Jul-06	0.2	0.425	0.469	
	28-Jul-06	4	0.38	0.461	
	29-Aug-06	0.2	0.685	0.785	
	29-Aug-06	3.8	0.647	0.948	
	28-Sep-06	0.2	0.483	0.664	
	28-Sep-06	3.5	0.456	0.594	
	01-Nov-06	0.2	0.532	0.57	
	01-Nov-06	3.9	0.494	0.896	
	21-Nov-06	0.2	0.307	0.414	
	21-Nov-06	3.7	0.292	0.466	
	07-Dec-06	0.2	0.366	0.63	
	07-Dec-06	3.5	0.64	0.732	
	20-Mar-07	0.2	0.477	0.664	
	20-Mar-07	4	0.572	0.714	
	26-Apr-07	0.2	0.49	0.759	
	26-Apr-07	4	0.702	0.865	
	23-May-07	0.2	0.526	0.644	
	23-May-07	4	0.607	0.658	
	26-Jun-07	0.2	0.816	0.681	
	26-Jun-07	4	0.702	0.729	
	24-Jul-07	0.2	0.669	0.705	
	24-Jul-07	3.5	0.622	0.751	
		Arithmetic average		0.50	0.63
		Geometric mean		0.48	0.61
		Median		0.49	0.66
		Standard deviation		0.16	0.16
	Geometric standard deviation		0.21	0.33	
	Lowest value		0.27	0.31	
	Highest value		0.82	0.95	

Table 2b. Total (RA) and dissolved (FA) selenium concentrations in water, site 2565.

Site	Sampling date	Depth (m)	FA (µg/L)	RA (µg/L)
	26-May-06	0.2	0.418	0.496
	19-Jun-06	0.2	0.245	0.396
	29-Jul-06	0.2	0.361	0.476
	29-Sep-06	0.2	0.391	0.646
	2-Nov-06	0.2	0.768	0.805
	22-Nov-06	0.2	0.291	0.416
	6-Dec-06	0.2	0.417	0.509
	20-Mar-07	0.2	0.361	0.656
	26-Apr-07	0.2	0.54	0.658
	23-May-07	0.2	0.547	0.64
	26-Jun-07	0.2	0.436	0.764
	25-Jul-07	0.2	0.708	0.651
	Arithmetic average		0.46	0.59
	Geometric mean		0.43	0.58
	Median		0.42	0.64
	Standard deviation		0.16	0.13
	Geometric standard deviation		1.38	1.25
2565 shallow	Lowest value		0.25	0.40
	Highest value		0.77	0.81
	26-May-06	6.5	0.366	0.504
	26-May-06	7.5	0.25	0.594
	19-Jun-06	6.5	0.205	0.446
	19-Jun-06	8	0.219	0.973
	29-Jul-06	6.5	0.25	0.25
	29-Jul-06	7.5	0.291	0.311
	29-Sep-06	6.5	0.401	0.484
	29-Sep-06	7.5	0.25	0.25
	2-Nov-06	6.5	0.584	0.643
	2-Nov-06	8	0.334	0.553
	22-Nov-06	6.5	0.25	0.25
	22-Nov-06	7.5	0.25	0.25
	6-Dec-06	6.5	0.377	0.502
	6-Dec-06	7.5	0.273	0.417
	20-Mar-07	6.5	0.463	0.682
	20-Mar-07	7.5	0.43	0.961
	26-Apr-07	6.5	0.507	0.825
	26-Apr-07	8	0.532	0.865
	23-May-07	6.5	0.632	0.709
	23-May-07	7.5	0.404	0.809
	26-Jun-07	6.5	0.433	0.616
	26-Jun-07	7.5	0.645	1.05
	25-Jul-07	6	0.574	0.864
	25-Jul-07	7	0.601	0.746
	Arithmetic average		0.40	0.61
	Geometric mean		0.37	0.55
	Median		0.39	0.61
	Standard deviation		0.14	0.25
	Geometric standard deviation		1.43	1.58
2565 deep	Lowest value		0.21	0.25
	Highest value		0.65	1.05

Table 2c. Total (RA) and dissolved (FA) selenium concentrations in water, site 3510.

Site	Sampling date	Depth (m)	FA (µg/L)	RA (µg/L)	
	23-May-06	0.2	0.461	0.605	
	20-Jun-06	0.2	0.363	0.479	
	27-Jul-06	0.2	0.335	0.437	
	1-Sep-06	0.2	0.586	0.779	
	29-Sep-06	0.2	0.452	0.534	
	4-Nov-06	0.2	0.559	0.665	
	21-Nov-06	0.2	0.334	0.522	
	7-Dec-06	0.2	0.452	0.623	
	19-Mar-07	0.2	0.59	0.671	
	1-May-07	0.2	0.843	0.8	
	31-May-07	0.2	0.591	0.746	
	27-Jun-07	0.2	0.506	0.613	
	25-Jul-07	0.2	0.62	0.642	
	Arithmetic average			0.51	0.62
	Geometric mean			0.50	0.61
Median			0.51	0.62	
Standard deviation			0.14	0.11	
Geometric standard deviation			1.29	1.19	
3510 shallow	Lowest value		0.33	0.44	
	Highest value		0.84	0.80	
3510 deep	23-May-06	6.5	0.409	0.642	
	23-May-06	8.5	0.292	0.716	
	20-Jun-06	7	0.348	0.477	
	20-Jun-06	8.5	0.243	0.654	
	27-Jul-06	7	0.248	0.411	
	27-Jul-06	8.5	0.35	0.417	
	1-Sep-06	6.5	0.745	0.777	
	1-Sep-06	8.5	0.461	1.14	
	29-Sep-06	6.5	0.431	0.526	
	29-Sep-06	8	0.25	0.251	
	4-Nov-06	6.5	0.408	0.576	
	4-Nov-06	8	0.349	0.548	
	21-Nov-06	6.5	0.478	0.723	
	21-Nov-06	8	0.549	0.551	
	7-Dec-06	6.5	0.378	0.47	
	7-Dec-06	8	0.25	0.523	
	19-Mar-07	6.5	0.544	0.674	
	19-Mar-07	8	0.681	0.812	
	1-May-07	6.5	0.622	0.806	
	1-May-07	8.5	0.468	0.718	
	31-May-07	7	0.569	0.916	
	31-May-07	8.3	0.593	0.718	
	27-Jun-07	7	0.571	0.712	
	27-Jun-07	8.1	0.453	0.723	
	25-Jul-07	6.5	0.662	0.736	
	25-Jul-07	8	0.618	0.76	
	Arithmetic average			0.46	0.65
Geometric mean			0.44	0.63	
Median			0.46	0.69	
Standard deviation			0.15	0.18	

Geometric standard deviation	1.40	1.35
Lowest value	0.24	0.25
Highest value	0.75	1.14

Table 2d. Total (RA) and dissolved (FA) selenium concentrations in water, site 2767.

Site	Sampling date	Depth (m)	FA (ppb)	RA (ppb)
	23-May-06	0.2	0.333	0.439
	23-May-06	3	0.364	0.412
	20-Jun-06	0.2	0.284	0.582
	20-Jun-06	3	0.319	0.418
	27-Jul-06	0.2	0.346	0.439
	27-Jul-06	3	0.33	0.449
	29-Aug-06	0.2	0.713	0.925
	29-Aug-06	2.7	0.762	0.844
	27-Sep-06	0.2	0.431	0.513
	27-Sep-06	2.2	0.538	0.626
	03-Nov-04	0.2	0.445	0.657
	20-Nov-06	0.2	0.281	0.46
	20-Nov-06	2.5	0.363	0.545
	07-Dec-06	0.2	0.432	0.464
	07-Dec-06	2.5	0.528	0.572
	19-Mar-07	0.2	0.626	0.677
	19-Mar-07	3	0.574	0.795
	02-May-07	0.2	0.546	0.699
	02-May-07	2.8	0.558	0.705
	31-May-07	0.2	0.545	0.625
	31-May-07	2.8	0.594	0.58
	28-Jun-07	0.2	0.522	0.845
	28-Jun-07	3	0.507	0.808
	24-Jul-07	0.2	0.662	0.68
	24-Jul-07	2.5	2.77	3.11
	Arithmetic average		0.57	0.71
	Geometric mean		0.50	0.64
	Median		0.52	0.63
	Standard deviation		0.48	0.52
	Geometric standard deviation		0.24	0.29
	Lowest value		0.28	0.41
2767	Highest value		2.77	3.11
Arith. average over total samples			0.49	0.64
Geometric mean over total samples			0.45	0.60
Median over total samples			0.46	0.64
Standard deviation over total samples			0.25	0.28
Geometric standard deviation over total samples			0.21	0.31
Lowest value			0.21	0.25
Highest value			2.77	3.11

Table 3a. Arithmetic average results (all water column sites and samples) for major and minor elements in shallow brine layer analyzed by ICP-MS. Total (RA) and dissolved (FA) results.

Element	Unit	Average for FA shallow brine	Average for RA shallow brine	Highest value FA/RA	Lowest value FA/RA
Li	mg/L	20.34 ± 0.80	20.79 ± 0.63	21.45 / 21.19	19.02 / 19.26
Na	mg/L	44891.18 ± 2004.37	46026.82 ± 1561.48	48231 / 47052	41841 / 42876
Mg	mg/L	4637.86 ± 205.44	4746.85 ± 160.21	4972.50 / 4847.40	4326.30 / 4397.40
S	mg/L	3377.62 ± 118.42	3415.25 ± 94.62	3522.60 / 3460.50	3188.70 / 3174.30
Cl	mg/L	85588.36 ± 2926.50	85968.00 ± 2384.21	89127 / 87183	81045 / 80154
K	mg/L	2603.86 ± 106.01	2654.35 ± 72.15	2685.60 / 2691.00	2402.10 / 2457.90
Ca	mg/L	270.23 ± 9.02	275.76 ± 5.78	283.14 / 283.68	258.93 / 265.14
Al	mg/L	14.52 ± 8.08	94.90 ± 35.61	26.45 / 127.80	4.65 / 21.86
Ti	µg/L	327.45 ± 14.10	338.75 ± 6.61	343.60 / 347.10	308.25 / 328.70
V	µg/L	6.06 ± 0.15	6.22 ± 0.08	6.54 / 6.37	6.02 / 6.15
Cr	µg/L	12.01 ± 0.97	12.23 ± 0.76	12.79 / 12.89	9.87 / 10.43
Mn	µg/L	20.97 ± 4.73	24.86 ± 3.54	25.63 / 26.81	13.95 / 17.94
Fe	µg/L	32.54 ± 18.61	95.50 ± 20.51	83.50 / 116.25	16.59 / 44.82
Co	µg/L	3.57 ± 0.03	3.62 ± 0.04	3.63 / 3.71	3.54 / 3.56
Ni	µg/L	4.42 ± 0.21	4.47 ± 0.12	4.78 / 4.65	4.13 / 4.17
Cu	µg/L	15.33 ± 1.52	15.50 ± 0.85	18.05 / 17.20	13.30 / 14.20
Zn	µg/L	15.20 ± 8.13	19.37 ± 16.82	31.85 / 64.50	4.68 / 6.58
As	µg/L	145.22 ± 9.98	147.44 ± 6.30	156.20 / 154.60	132.45 / 131.60
Sr	µg/L	2469.09 ± 107.58	2536.41 ± 58.01	2589.50 / 2598.00	2310.00 / 2428.00
Mo	µg/L	44.75 ± 3.20	46.13 ± 1.92	51.20 / 50.15	42.29 / 43.95
Cd	µg/L	2.60 ± 0.21	2.65 ± 0.33	2.80 / 3.08	2.12 / 1.88
Sb	µg/L	15.43 ± 0.71	15.67 ± 0.64	16.33 / 16.63	14.50 / 14.98
Ba	µg/L	124.67 ± 1.97	130.71 ± 2.64	126.85 / 133.70	120.50 / 126.80
Tl	µg/L	1.78 ± 0.04	1.77 ± 0.02	1.84 / 1.79	1.71 / 1.73
Pb	µg/L	3.41 ± 0.28	3.66 ± 0.24	3.98 / 4.01	3.04 / 3.10
U	µg/L	9.34 ± 0.41	9.55 ± 0.19	9.93 / 9.87	8.87 / 9.33

Table 3b. Geometric mean and median (all water column sites and samples) for major and minor elements in shallow brine layer analyzed by ICP-MS. Total (RA) and dissolved (FA) results

Element	Units	Geometric mean -Shallow		Median - Shallow	
		FA	RA	FA	RA
Li	mg/L	19.8	20.1	19.76	19.84
Na	mg/L	43707.9	44514.9	43245.00	43830.00
Mg	mg/L	4502.2	4583.3	4440.15	4509.00
S	mg/L	3302.8	3324.2	3296.70	3310.20
Cl	mg/L	83832.7	83887.4	83785.50	83245.50
K	mg/L	2541.8	2575.2	2553.75	2580.75
Ca	mg/L	268.3	272.8	268.02	270.59
Al	mg/L	12.3	85.6	12.12	98.58
Ti	µg/L	324.6	335.9	328.60	333.68
V	µg/L	6.1	6.2	6.07	6.18
Cr	µg/L	11.6	11.9	11.57	12.00
Mn	µg/L	17.9	21.9	17.89	21.40
Fe	µg/L	30.4	80.8	27.97	87.58
Co	µg/L	3.6	3.6	3.56	3.61
Ni	µg/L	4.4	4.4	4.41	4.46
Cu	µg/L	15.6	15.5	15.50	15.69
Zn	µg/L	13.9	16.4	14.38	14.51
As	µg/L	143.8	147.3	144.60	147.33
Sr	µg/L	2431.3	2519.7	2463.25	2521.25
Mo	µg/L	45.8	47.0	45.54	46.75
Cd	µg/L	2.5	2.5	2.54	2.59
Sb	µg/L	15.3	15.8	15.4	15.7
Ba	µg/L	123.7	129.6	124.5	129.1
Tl	µg/L	1.8	1.8	1.77	1.76
Pb	µg/L	3.5	3.6	3.59	3.64
U	µg/L	9.3	9.5	9.3425	9.46

Table 3c. Arithmetic average results for major and minor elements in deep brine layer (all water column sites and samples) analyzed by ICP-MS. Total (RA) and dissolved (FA) results

Element	Unit	Average for FA deep brine	Average for RA deep brine	Highest value FA/RA	Lowest value FA/RA
Li	mg/L	25.84 ± 5.61	26.15 ± 5.82	35.84 / 37.36	20.08 / 20.56
Na	mg/L	55920.38 ± 11944.08	56787.75 ± 12591.38	78561 / 81567	43812 / 44604
Mg	mg/L	5857.31 ± 1315.12	5927.74 ± 1369.95	8297.10 / 8518.50	4465.8 / 4574.7
S	mg/L	4255.99 ± 925.75	4207.50 ± 883.04	5979.60 / 5762.70	3282.3 / 3301.2
Cl	mg/L	106984.13 ± 23324.56	105842.25 ± 22193.84	152370 / 145620	81810 / 82656
K	mg/L	3275.10 ± 667.25	3309.98 ± 683.16	4508.10 / 4631.40	2577.6 / 2667.6
Ca	mg/L	293.48 ± 21.34	299.89 ± 22.80	325.26 / 335.52	268.74 / 278.19
Al	mg/L	344.48 ± 940.88	899.50 ± 1248.80	2673.00 / 3491.50	6.68 / 15.71
Ti	µg/L	374.11 ± 46.87	397.17 ± 67.83	475.55 / 538.50	328.95 / 330.75
V	µg/L	5.96 ± 1.89	7.41 ± 1.92	10.34 / 11.59	4.28 / 6.17
Cr	µg/L	14.78 ± 3.34	14.90 ± 3.29	20.34 / 20.43	10.84 / 11.26
Mn	µg/L	54.73 ± 34.96	64.75 ± 44.88	124.45 / 147.40	22.61 / 26.74
Fe	µg/L	227.75 ± 566.46	592.99 ± 706.55	1629.50 / 2040.00	17.04 / 48.79
Co	µg/L	3.64 ± 0.34	3.88 ± 0.41	4.47 / 4.76	3.40 / 3.54
Ni	µg/L	5.55 ± 1.67	5.52 ± 1.36	9.08 / 8.29	4.44 / 4.34
Cu	µg/L	16.21 ± 5.08	19.26 ± 6.29	27.13 / 31.97	11.33 / 15.02
Zn	µg/L	18.54 ± 8.66	18.32 ± 8.43	31.72 / 29.84	7.66 / 8.36
As	µg/L	163.69 ± 18.59	163.16 ± 16.65	206.80 / 192.95	149.55 / 146.65
Sr	µg/L	2816.38 ± 247.83	2797.75 ± 228.39	3199.00 / 3143.50	2509 / 2492
Mo	µg/L	33.54 ± 13.85	39.92 ± 9.41	49.28 / 52.00	13.29 / 29.43
Cd	µg/L	3.25 ± 0.55	3.08 ± 0.64	4.15 / 4.06	2.45 / 2.24
Sb	µg/L	16.43 ± 0.95	16.27 ± 1.22	17.75 / 17.76	15.01 / 14.55
Ba	µg/L	135.02 ± 13.80	145.30 ± 17.38	165.21 / 173.73	123.16 / 124.81
Tl	µg/L	1.91 ± 0.27	1.88 ± 0.12	2.56 / 2.02	1.73 / 1.71
Pb	µg/L	4.23 ± 3.56	6.90 ± 4.51	12.98 / 16.20	2.42 / 3.61
U	µg/L	9.51 ± 0.34	9.67 ± 0.35	9.89 / 10.14	8.88 / 9.11

Table 3d. Geometric mean and median (all water column sites and samples) for major and minor elements in deep brine layer analyzed by ICP-MS. Total (RA) and dissolved (FA) results

	Units	Geometric mean-Shallow		Median - Shallow	
		FA	RA	FA	RA
Li	mg/L	25.8	26.2	25.3	25.6
Na	mg/L	55920.4	56787.8	54871.2	55664.2
Mg	mg/L	5857.3	5927.7	5734.7	5798.3
S	mg/L	4256.0	4207.5	4172.3	4130.0
Cl	mg/L	106984.1	105842.3	104908.9	103906.3
K	mg/L	3275.1	3310.0	3218.3	3252.6
Ca	mg/L	293.5	299.9	292.8	299.1
Al	mg/L	344.5	899.5	21.5	297.4
Ti	µg/L	374.1	397.2	371.8	392.6
V	µg/L	6.0	7.4	5.7	7.2
Cr	µg/L	14.8	14.9	14.5	14.6
Mn	µg/L	54.7	64.7	46.0	53.1
Fe	µg/L	227.7	593.0	44.0	281.3
Co	µg/L	3.6	3.9	3.6	3.9
Ni	µg/L	5.5	5.5	5.4	5.4
Cu	µg/L	16.2	19.3	15.6	18.5
Zn	µg/L	18.5	18.3	16.7	16.6
As	µg/L	163.7	163.2	162.9	162.4
Sr	µg/L	2816.4	2797.8	2806.8	2789.7
Mo	µg/L	33.5	39.9	30.8	39.0
Cd	µg/L	3.3	3.1	3.2	3.0
Sb	µg/L	16.4	16.3	16.4	16.2
Ba	µg/L	135.0	145.3	134.5	144.4
Tl	µg/L	1.9	1.9	1.9	1.9
Pb	µg/L	4.2	6.9	3.5	5.9
U	µg/L	9.5	9.7	9.5	9.7

Table 4a. Volatile selenium concentration in the Great Salt Lake

Date	Site	Depth (m)	[Se] (ng/L)	[Se] (pmol/L)
9/1/06	3510	0.2	1.1	10.1
9/1/06	3510	1.5	1.9	17.5
9/1/06	3510	8.5	0.6	5.2
9/11/06	GS-5	7.5	6.4	58.5
9/12/06	GS-11	8	1.8	16.3
9/12/06	GS-20	7	0.3	2.4
9/12/06	3510	0.2	5.3	48.4
9/27/06	2267	0.2	0.1	1.0
9/27/06	2267	3.5	3.3	30.6
9/27/06	2767	0.2	1.1	9.6
9/27/06	2767	2.2	1.4	12.4
9/28/06	2565	0.2	9.2	84.3
9/28/06	2565	8	1.7	15.4
9/28/06	3510	0.2	1.5	13.6
9/28/06	3510	8	0.2	1.7
September	Average		2.4	21.8
	Standard deviation		2.6	24.0
	Lowest value		0.1	1.0
	Highest value		9.2	84.3
11/1/06	2565	6.5	3.0	27.2
11/3/06	3510	0.2	6.4	58.9
11/3/06	3510	6.5	0.4	3.7
11/16/06	GS-9	2.5	3.1	28.2
11/16/06	GS-5	2	2.4	21.8
11/17/06	GS-20	2.5	0.4	3.4
11/17/06	GS-18	7.7	1.8	16.6
11/17/06	GS-14	7	0.6	6.0
11/17/06	GS-12	5	3.4	31.6
11/20/06	3510	3	1.7	15.5
11/20/06	3510	7	0.0	0.2
11/20/06	2767	2	1.3	11.6
11/21/06	2267	1	1.7	15.2
11/21/06	2565	8	0.6	5.9
11/21/06	2565	0.2	1.3	12.0
November	Average		1.9	17.2
	Standard deviation		1.6	15.0
	Lowest value		0.0	0.2
	Highest value		6.4	58.9

Table 4b. Volatile selenium concentration in the Great Salt Lake

Date	Site	Depth (m)	[Se] (ng/L)	[Se] (pmol/L)
12/6/06	2565	0.5	0.0	0.4
12/6/06	2565	4	0.0	0.4
12/6/06	2767	0.5	0.0	0.4
12/6/06	2767	2.5	1.2	10.6
12/7/06	3510	0.5	0.2	1.6
12/7/06	3510	8	0.0	0.4
12/7/06	2267	0.5	0.0	0.4
12/7/06	2267	3	1.0	8.9
December	Average		0.3	2.9
	Standard deviation		0.5	4.3
	Lowest value		0.0	0.4
	Highest value		1.2	10.6
5/1/07	3510	0.2	7.1	65.4
5/1/07	3510	3	0.0	0.4
5/1/07	3510	4.5	0.0	0.4
5/1/07	3510	6.5	0.0	0.4
5/1/07	3510	8.5	0.3	2.3
5/10/07	2565	0.2	0.3	2.6
5/10/07	2565	3	1.9	17.8
5/10/07	2565	6.5	9.1	83.3
5/10/07	2565	7.5	0.5	4.6
May	Average		2.1	19.7
	Standard deviation		3.5	31.8
	Lowest value		0.0	0.4
	Highest value		9.1	83.3
6/1/07	3510	0.5	0.0	0.4
6/1/07	3510	4	8.5	78.3
6/1/07	3510	5	0.9	8.3
6/1/07	3510	6.5	3.0	27.4
6/1/07	3510	8	0.0	0.4
6/27/07	3510	0.2	0.0	0.4
6/27/07	3510	3	1.6	15.0
6/27/07	3510	5	4.3	39.7
6/27/07	3510	7	0.1	0.8
6/27/07	3510	8	0.2	2.2
June	Average		1.9	17.3
	Standard deviation		2.8	25.3
	Lowest value		0.0	0.4
	Highest value		8.5	78.3

Table 4c. Volatile selenium concentration in the Great Salt Lake

Date	Site	Depth (m)	[Se] (ng/L)	[Se] (pmol/L)
7/2/07	2267	0.2	1.6	14.8
7/2/07	2267	1	1.7	15.4
7/2/07	2267	2	4.1	37.5
7/2/07	2267	3.5	22.7	208.1
7/26/07	2267	0.2	4.6	41.9
7/26/07	2267	1.5	6.1	56.0
7/26/07	2267	2.5	7.8	71.3
7/26/07	2267	3.5	17.0	156.1
7/27/07	2565	0.2	0.1	0.6
7/27/07	2565	3	2.2	20.2
7/27/07	2565	5	7.7	70.2
7/27/07	2565	6.5	13.3	122.3
7/27/07	2565	7.5	0.6	5.1
July	Average		6.9	63.0
	Standard deviation		6.9	63.4
	Lowest value		0.1	0.6
	Highest value		22.7	208.1
8/24/07	2767	0.2	4.5	41.7
8/24/07	2767	1	2.3	21.1
8/24/07	2767	2	0.8	7.7
8/30/07	3510	0.2	3.4	31.0
8/30/07	3510	3	10.0	91.7
8/30/07	3510	5	17.8	163.5
8/30/07	3510	7	0.4	3.6
8/30/07	3510	8	0.0	0.4
August	Average		4.9	45.1
	Standard deviation		6.1	56.2
	Lowest value		0.0	0.4
	Highest value		17.8	163.5
Average over total samples			3.0	27.4
Geometric mean			0.9	8.2
Standard deviation over total samples			4.4	39.9
Lowest value over total samples			0.0	0.2
Highest value over total value			22.7	208.1

Table 5. Volatile selenium diffusive flux

Date	Site	Depth (m)	ngSe/L	T(°C)	D _{DMS} (cm ² /s)	J (g Se/cm ² /yr)	Flux (Kg/yr)
9/1/06	3510	0.2	0.37	22.15	1.2E-05	5.4E-13	9.9E-03
		1.5	0.55				
9/27/06	2267	0.2	0.14	16.4	1.0E-05	7.2E-13	1.3E-02
		3.5	0.87				
9/27/06	2767	0.2	0.36	16.4	1.0E-05	1.1E-13	2.1E-03
		2.2	0.43				
12/6/06	2767	0.5	0.04	8.48	8.4E-06	4.5E-13	8.3E-03
		2.5	0.38				
12/6/06	2565	0.5	0.02	8.48	8.4E-06	4.7E-14	8.6E-04
		4	0.09				
12/7/06	2267	0.5	0.09	8.48	8.4E-06	2.6E-13	4.7E-03
		3	0.34				
5/10/07	2565	0.2	0.18	17.87	1.1E-05	4.4E-13	8.2E-03
		3	0.56	16.28	1.0E-05	1.5E-12	2.7E-02
		6.5	2.17	13.78			
6/1/07	3510	0.5	0.091	20.55	1.1E-05	1.8E-13	3.4E-03
		5	0.322	19.36	1.1E-05	1.1E-12	2.0E-02
		6.5	0.794	18.51			
6/27/07	3510	0.2	0.05	24.71	1.3E-05	6.3E-13	1.2E-02
		3	0.49	23.59	1.2E-05	1.2E-12	2.2E-02
		5	1.10	23.04			
7/2/07	2267	0.2	0.484	25.53	1.3E-05	7.8E-14	1.4E-03
		1	0.499	25.53	1.3E-05	2.2E-12	4.1E-02
		2	1.042	25.37	1.3E-05	1.2E-11	2.2E-01
		3.5	5.244	26.74			
7/26/07	2267	0.2	1.151	27.09	1.4E-05	1.1E-12	2.1E-02
		1.5	1.499	27.19	1.4E-05	1.6E-12	3.0E-02
		2.5	1.874	27.45	1.4E-05	9.0E-12	1.7E-01
		3.5	3.964	27.67			
7/27/07	2565	0.2	0.1	27.67	1.4E-05	3.3E-12	6.0E-02
		3	2.2	27.14	1.4E-05	1.2E-11	2.2E-01
		5	7.7	27.06	1.3E-05	1.6E-11	2.9E-01
		6.5	13.3	26.02			
8/30/07	3510	0.2	3.4	27.67	1.4E-05	1.0E-11	1.9E-01
		3	10.0	27.14	1.4E-05	1.7E-11	3.1E-01
		5	17.8	27.06			
Average					1.2E-05	3.9E-12	7.3E-02

Table 6a. Estimated water transfer velocities (k_w), volatile selenium fluxes, using an average volatile selenium concentration of 0.52 ng/L in water.

Estuarine model			
Wind velocity: 5 miles/h (2.2 m/s)			
T(°C)	k_w (cm/h)	Flux (gSe/cm²/yr)	Flux (Kg Se/yr)
2	1.58	4.2E-08	766
6	1.77	4.6E-08	856
10	1.98	5.2E-08	956
17	2.38	6.2E-08	1150
28	3.06	8.0E-08	1480
Wind velocity: 25 miles/h (11.2 m/s)			
T(°C)	k_w (cm/h)	Flux (gSe/cm²/yr)	Flux (Kg Se/yr)
2	16.07	4.2E-07	7780
6	17.96	4.7E-07	8695
10	20.06	5.3E-07	9710
17	24.12	6.3E-07	11676
28	31.05	8.2E-07	15030
Modified Liss & Merlivat model			
Wind velocity: 5 miles/h (2.2 m/s)			
T(°C)	k_w (cm/h)	Flux (gSe/cm²/yr)	Flux (Kg Se/yr)
2	2.05	2.4E-08	450
6	2.37	2.8E-08	522
10	2.75	3.3E-08	605
17	3.52	4.2E-08	774
28	4.92	5.9E-08	1083
Wind velocity: 25 miles/h (11.2 m/s)			
T(°C)	k_w (cm/h)	Flux (gSe/cm²/yr)	Flux (Kg Se/yr)
2	11.12	2.9E-07	5381
6	12.42	3.3E-07	6013
10	13.87	3.6E-07	6715
17	16.68	4.4E-07	8076
28	21.47	5.6E-07	10395

Table 6b. Results of measured volatile Se fluxes compared to Estuarine model predicted fluxes with environmental parameters used in calculations.

Sample ID	Site	Date	Avg. Wind Velocity m/s	Surface Temp. °C	Vol. Se Conc. ng/L	Measured Flux ng/m²h	Estuarine Predicted Flux ng/m²h
1B	3510	6/1/07	2.63	20.55	0.06	11.12	1.80
1C	3510	6/27/07	3.74	24.71	0.05	2.08	2.41
2C	2267	7/2/07	1.25	25.53	1.43	20.13	31.13
3C	2267	7/26/07	1.34	27.09	4.43	9.38	102.10
4C	2565	7/27/07	1.86	27.67	0.20	3.23	5.43

Table 6c. Summary of errors associated to different parameters used to calculate the volatilization flux of Se to the atmosphere.

Parameter	Error	Reference
Temperature (°C)	0.5	Crosman & Horel, 2006
Wind velocity (m/s)	2.5	Horel, 2007
$C_{water}^{1/Se}$ (ng/L)	7.7	Geometric standard deviation
Area GSL (acres)	427.2	Average of calculated area difference per 0.1 foot in depth

Table 7a Results of shallow (only) sediment trap analyses at site 2267

Average month	Days acum.	Average sediment weight (g)	Downward flux (g/cm ² /year)	[Se] (mg/Kg)	Se downward flux (gSe/cm ² /yr)
Apr-06	64	18.22	2.55	0.27	6.76E-07
Jun-06	24	8.81	3.29	1.54	5.07E-06
Jul-06	39	18.21	4.19	0.31	1.30E-06
Jul-06	32	9.96	2.79	0.20	5.58E-07
Sep-06	64	24.76	3.47	0.33	1.13E-06
Nov-06	36	8.49	2.12	0.20	4.23E-07
Jan-07	103	8.82	0.77	1.16	8.94E-07
Apr-07	37	21.65	5.25		
Jun-07	34	8.13	2.14		
Average			2.95	0.57	1.44E-06
Accumulative	433	127.06	2.63		

n/a – not available

Table 7b Results of deep sediment trap analyses at site 2565

Average month	Days acum.	Average sediment weight (g)	Downward flux (g/cm ² /year)	[Se] (mg/Kg)	Se downward flux (gSe/cm ² /yr)
Apr-06	64	14.29	2.00	0.02	3.00E-08
Jun-06	24	0.86	0.32	1.70	5.48E-07
Jul-06	39	0.00	0.00	n/a	n/a
Aug-06	45	0.55	0.11	1.67	1.83E-07
Oct-06	51	1.26	0.22	0.23	5.09E-08
Jan-07	139	1.24	0.08	0.51	4.04E-08
Apr-07	37	1.79	0.43	0.15	6.50E-08
Jun-07	42	5.02	1.07		
Average			0.53	0.71	1.53E-07
Accumulative	441	25.01	0.51		

n/a – not available

Table 7c Results of shallow sediment trap analyses at site 2565

Average month	Days acum.	Average sediment weight (g)	Downward flux (g/cm ² /year)	[Se] (mg/Kg)	Se downward flux (gSe/cm ² /yr)
Apr-06	64	0.000	0.000	n/a	n/a
Jun-06	24	0.000	0.000	n/a	n/a
Jul-06	39	0.000	0.000	n/a	n/a
Aug-06	45	0.169	0.034	1.279	4.30E-08
Oct-06	51	0.000	0.000	n/a	n/a
Jan-07	139	0.853	0.055	0.558	3.07E-08
Apr-07	37	0.512	0.124	0.445	5.52E-08
Jun-07	42	0.301	0.064		
Average			0.035	0.761	4.30E-08
Accumulative	441	1.834	0.037		

n/a – not available

Table 7d Results of deep sediment trap analyses at site 3510

Average month	Days acum.	Average sediment weight (g)	Downward flux (g/cm ² /year)	[Se] (mg/Kg)	Se downward flux (gSe/cm ² /yr)
Jul-06	30	3.61	1.08	0.01	1.08E-08
Aug-06	47	0.08	0.02	0.87	1.41E-08
Oct-06	52	0.85	0.15	0.18	2.55E-08
Nov-06	34	0.00	0.00	n/a	n/a
Jan-07	101	1.09	0.10	0.70	6.82E-08
Jun-07	28	2.35	0.75	0.10	7.52E-08
Average			0.35	0.31	3.88E-08
Accumulative	292	7.98	0.25		

n/a – not available

Table 7e Results of shallow sediment trap analyses at site 3510

Average month	Days acum.	Average sediment weight (g)	Downward flux (g/cm²/year)	[Se] (mg/Kg)	Se downward flux (gSe/cm²/yr)
Jul-06	30	0.00	0.000	n/a	n/a
Aug-06	47	0.10	0.020	1.44	2.85E-08
Oct-06	52	0.35	0.061	0.20	1.19E-08
Nov-06	34	0.00	0.000	n/a	n/a
Jan-07	101	0.82	0.072	0.76	5.50E-08
Jun-07	28	0.79	0.252	< 0.01	< 2.52E-09
Average			0.068	0.40	3.18E-08
Accumulative	292	2.06	0.063		

n/a – not available

Table 8. Average Se concentration below 5 cm. in cores

Core ID	Se Conc. (ug/g)
2267-2	0.53
2565-3	0.53
3510 Box Core	0.94
DD-C	1.96
DD-I	1.42
DD-L	0.69
DD-Q	0.50
DD-R	1.06
<i>Average</i>	<i>0.95</i>

Table 9. Average mass accumulation rate (MAR) in each core

Core ID	MAR (g/cm ² /yr)
DD-C	0.036
DD-I	0.049
DD-R	0.027
DD-L	0.025
DD-Q	0.010
3510	0.043
<i>Average</i>	<i>0.032</i>

Table 10. Average below-5-cm Se concentration, MAR, area, and calculated mass of selenium removed annually within each sedimentation zone

Sed. Zone	Avg. [Se] (ug/g)	Estimated MAR (g/cm ² /yr)	Area (km ²)	Estimated Mass of Se Removed (kg/yr)
Very Low	0.53	0.009	1251.6	59.70
Low	0.82	0.018	420.9	62.12
Medium	0.9	0.026	358.5	83.89
High	1.96	0.04	47.9	37.55
Very High	1.96	0.05	4.6	4.51
Total				247.78

Table 11. Estimation of error of MAR for each sedimentation zone and range of mass of Se removed annually by sedimentation.

Sed. Zone	Avg. [Se] (ug/g)	Estimated MAR (g/cm ² /yr)	High MAR (x2) (g/cm ² /yr)	Low MAR (/2) (g/cm ² /yr)	Area (km ²)	Estimated Mass of Se Removed (kg/yr)	High Mass of Se Removed (kg/yr)	Low Mass of Se Removed (kg/yr)
Very Low	0.53	0.009	0.018	0.0045	1251.6	59.70	119.40	29.85
Low	0.82	0.018	0.036	0.009	420.9	62.12	124.25	31.06
Medium	0.9	0.026	0.052	0.013	358.5	83.89	167.78	41.94
High	1.96	0.04	0.08	0.02	47.9	37.55	75.11	18.78
Very High	1.96	0.05	0.1	0.025	4.6	4.51	9.02	2.25
Total						247.78	495.55	123.89

Table 12. Low, medium and high fluxes used in the removal processes distribution

	LOW FLUXES (Kg/yr)	MEDIUM FLUXES (Kg/yr)	HIGH FLUXES (Kg/yr)
Volatilization	357.3	2108	12437
Permanent sedimentation	124	248	496
Brine shrimp harvesting	28	28	28
TOTAL	509.3	2384	12961

Table 13. Estimated values for wet and dry Se atmospheric deposition flux at different locations.

	Estimated Se atmospheric deposition flux	Reference
Wet depositional flux, Bermuda ($\mu\text{mol}/\text{m}^2/\text{yr}$)	0.42	Cutter&Cutter, 1998
Wet depositional flux, Mace Head, Ireland ($\mu\text{mol}/\text{m}^2/\text{yr}$)	0.78	Cutter&Cutter, 1998
Total (wet+dry) deposition, Amazon River ($\text{nmol}/\text{m}^2/\text{yr}$)	1772	Cutter&Cutter, 2001
Wet deposition, Barbados ($\text{nmol}/\text{m}^2/\text{yr}$)	1440	Cutter&Cutter, 2001
Lake Superior, dry deposition ($\mu\text{g}/\text{m}^2/\text{yr}$)	52	Sweet et al, 1998
Lake Superior, wet deposition ($\mu\text{g}/\text{m}^2/\text{yr}$)	520	Sweet et al, 1998
Lake Michigan, dry deposition ($\mu\text{g}/\text{m}^2/\text{yr}$)	52	Sweet et al, 1998
Lake Michigan, wet deposition ($\mu\text{g}/\text{m}^2/\text{yr}$)	520	Sweet et al, 1998
Lake Erie, dry deposition ($\mu\text{g}/\text{m}^2/\text{yr}$)	95	Sweet et al, 1998
Lake Erie wet deposition ($\mu\text{g}/\text{m}^2/\text{yr}$)	630	Sweet et al, 1998
Chesapeake Bay- average, dry deposition ($\mu\text{g}/\text{m}^2/\text{yr}$)	259	Baker et al, 1994
Chesapeake Bay- average, wet deposition ($\mu\text{g}/\text{m}^2/\text{yr}$)	130	Baker et al, 1994
Chesapeake Bay- average- total deposition ($\mu\text{g}/\text{m}^2/\text{yr}$)	389	Baker et al, 1994